Structural and Biochemical Investigation of the Heterodimeric Murine tRNA-Guanine Transglycosylase

Maurice Sebastiani, Christina Behrens, Stefanie Dörr, Hans-Dieter Gerber, Rania Benazza, Oscar Hernandez-Alba, Sarah Cianférani, Gerhard Klebe, Andreas Heine, Klaus Reuter

Structural and Biochemical Investigation of the Heterodimeric Murine tRNA-Guanine Transglycosylase

Maurice Sebastiani[§], Christina Behrens[§], Stefanie Dörr[§], Hans-Dieter Gerber[§], Rania Benazza[†¥], Oscar Hernandez-Alba[†¥], Sarah Cianférani[†¥], Gerhard Klebe[§], Andreas Heine[§], Klaus Reuter[§]*

[§]Institut für Pharmazeutische Chemie, Philipps-Universität Marburg, Marbacher Weg 8, D-35037 Marburg, Germany

[†]Laboratoire de Spectrométrie de Masse BioOrganique, Université de Strasbourg, CNRS, IPHC UMR 7178, 67000 F-Strasbourg, France

[¥]Infrastructure Nationale de Protéomique ProFI – FR2048, 67087 Strasbourg, France

*To whom correspondence should be addressed

Email address of the corresponding author: reuterk@staff.uni-marburg.de

ABSTRACT

In $tRNA^{Asp}$, $tRNA^{Asn}$, $tRNA^{Tyr}$ and $tRNA^{His}$ of most bacteria and eukaryotes the anticodon wobble position may be occupied by the modified nucleoside queuosine, which affects the speed and the accuracy of translation. Since eukaryotes are not able to synthesize queuosine de novo, they have to salvage queuine (the queuosine base) as a micronutrient from food and/or the gut microbiome. The heterodimeric Zn^{2+} containing enzyme tRNA-guanine transglycosylase (TGT) catalyzes the insertion of queuine into the above-named tRNAs in exchange for the genetically encoded guanine. This enzyme has attracted medical interest since it was shown to be potentially useful for the treatment of multiple sclerosis. In addition, TGT inactivation via gene knockout leads to suppressed cell proliferation and migration of certain breast cancer cells, which may render this enzyme a potential target for the design of compounds supporting breast cancer therapy. As a prerequisite to fully exploit the medical potential of eukaryotic TGT, we have determined and analyzed a number of crystal structures of the functional murine TGT with and without bound queuine. In addition, we have investigated the importance of two residues of its non-catalytic subunit on dimer stability and determined the Michaelis-Menten parameters of murine TGT with respect to tRNA and several natural as well as artificial nucleobase substrates. Ultimately, on the basis of available TGT crystal structures, we provide an entirely conclusive reaction mechanism for this enzyme, which in detail explains why the TGT-catalyzed insertion of some nucleobases into tRNA occurs reversibly while that of others is irreversible.

INTRODUCTION

In $tRNA^{Asp}$, $tRNA^{Asn}$, $tRNA^{Tyr}$ and $tRNA^{His}$ of most bacteria and eukaryotes, the anticodon wobble position (position 34) is occupied by the 7-deazaguanosine derivative queuosine (for structural formula of the nucleobase see Figure 1), which is involved in the fine-tuning of translational speed and accuracy.[1] Furthermore, in eukaryotes, the queuosine modification reduces the sensitivity of tRNA against the stress-induced RNase angiogenin[2] and is prerequisite for the efficient methylation of cytidine-38 of $tRNA^{Asp}$ by the methyltransferase Dnmt2.[3] The biosynthesis of queuosine is unique to bacteria. Via a series of five enzyme-catalyzed reactions, it starts outside the tRNA with GTP being converted to 7-(aminomethyl)-7-deazaguanine, also referred to as $preQ_1$ base.[4-8] In the next step, the enzyme tRNA-guanine transglycosylase (TGT; EC 2.4.2.29) catalyzes the insertion of this intermediate into tRNA, which occurs in exchange for the genetically encoded guanine.[9] Thereupon, at the tRNA level and mediated by the enzyme tRNA $preQ_1$-34 *S*-adenosylmethionine ribosyltransferase-isomerase (QueA), the exocyclic aminomethyl group of $preQ_1$ is endowed with an epoxy-dihydroxy-cyclopentyl moiety originating from the ribose of *S*-adenosyl-L-methionine.[10,11] Eventually, the epoxide within the attached five-membered ring is reduced to a double bond by the enzyme epoxyqueuosine reductase.[12,13]

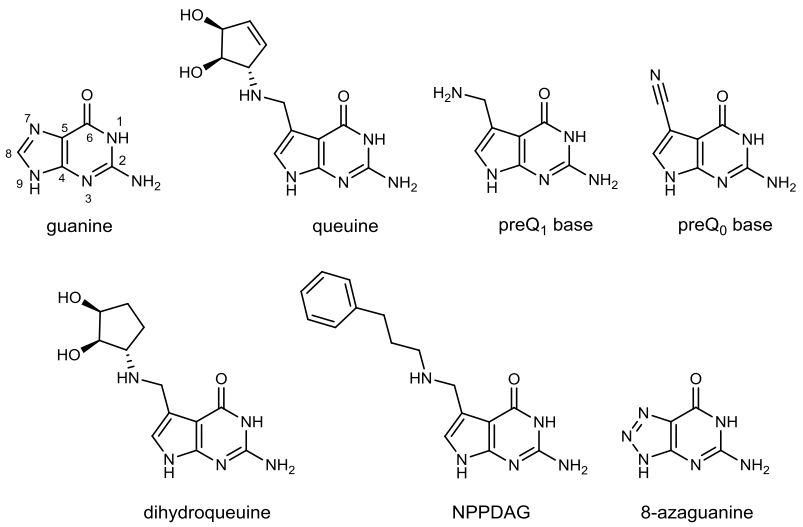

Figure 1. Substrate bases of murine TGT used in this study. A cyclopentenediol moiety originating from the ribose of *S*-adenosyl-L-methionine is attached to the aminomethyl group of queuine, the physiological substrate of the eukaryotic TGT. This substituent is missing in the $preQ_1$ base, the physiological substrate of the bacterial TGT. The figure was created by the program *ChemDraw*® (version 18.2.0.48).

Facilitated by the high-resolution crystal structure of the TGT from *Zymomonas mobilis*,[14] the bacterial TGT has been well investigated. It constitutes a homodimer with each subunit featuring a $(\beta\alpha)_8$ barrel fold extended by a three-stranded antiparallel β sheet at its N-terminus and by an extra α helix at its C-terminus. In addition, the non-canonical barrel harbors several insertions, the most prominent being a Zn^{2+}-coordinating subdomain, which is a substantial component of the dimer interface. Although each TGT subunit contains a functional active center, the homodimer can accommodate only one tRNA substrate at a time since the simultaneous binding of two such bulky molecules would lead to extensive clash.[15,16] Certainly, both monomers of the active complex are necessary to efficiently bind the tRNA substrate and to align it in the correct orientation which is required for catalysis.

Except for the TGT, eukaryotes do not possess any enzyme specific for queuosine biosynthesis and, therefore, are not able to produce this modified nucleoside de novo. Hence, animals as well as human have to salvage queuine (the queuosine base) from food and/or from the gut microbiome. Accordingly, instead of the $preQ_1$ base, the eukaryotic TGT (EC 2.4.2.64) has to accept queuine as a substrate in order to insert it into position 34 of $tRNA^{Asp}$, $tRNA^{Asn}$, $tRNA^{Tyr}$ and $tRNA^{His}$. In contrast to its bacterial counterpart, the eukaryotic TGT is a heterodimer with both of its subunits, QTRT1 and QTRT2, closely resembling the bacterial TGT monomer.[17-20] Yet, only QTRT1 is endowed with an active center while the non-catalytic QTRT2 obviously supports the potent binding and the correct orientation of the tRNA substrate.

Since it is known that a functional TGT is essential for the pathogenicity of *Shigella* bacteria, the causative agents of bacillary dysentery,[21] we use the bacterial TGT as a target for the rational design of compounds with therapeutic potential against Shigellosis. Yet, it was shown that, in mice, the genetic inactivation of the TGT leads to the uncontrolled oxidation of tetrahydrobiopterin, the cofactor of aromatic amino acid hydroxylases and of nitric oxide synthase.[22] On this account, it seems desirable to create compounds which inhibit the bacterial TGT but not the human one. Therefore, we became interested in the eukaryotic TGT, because, for this purpose, we deemed detailed structural

and biochemical knowledge on the eukaryotic enzyme essential. Meanwhile, however, a number of studies have been published which show that the medical relevance of the eukaryotic TGT goes still further.

For example, Varghese et al. reported that the synthetic 7-deazaguanine derivative "NPPDAG" rapidly and completely removes the symptoms elicited by "experimental autoimmune encephalomyelitis", a murine model of multiple sclerosis. The remission of disease is caused by an anti-proliferating influence of NPPDAG on antigen-specific effector memory T cells and central memory T cells (but not naïve T cells). Obviously, this effect relies on the TGT-catalyzed insertion of NPPDAG into tRNA since it does not appear in *QTRT1* knockout mice.[23] Moreover, Zhang et al. provided evidence that the knockout of the *QTRT1* gene leads to suppressed cell proliferation and migration of breast cancer-derived MCF-7 cells. Consistently, in a xenograft nude mouse model they observed substantially reduced number, volume and weight of tumors in mice injected with *QTRT1*-knockout MCF-7 cells compared to wild type MCF-7 cells.[24] This may render mammalian TGT a potential target for the design of compounds which might support the treatment of certain types of breast cancer. In addition, Nagaraja et al. revealed evidence that the presence of queuine provides elevated stress resistance to *Entamoeba histolytica*, the causative agent of amebiasis. However, this effect, which will not appear if *QTRT1* expression is silenced via antisense small RNAs, is concomitant with the reduced pathogenicity of this organism.[25] Ultimately, the mitochondrial genome of the protozoan parasite *Trypanosoma brucei* does not contain a single tRNA gene, which is why in this organism all tRNAs have to be imported into mitochondria from the cytoplasm. Kulkarni et al. showed that, in the absence of the queuosine modification, the import of $tRNA^{Asp}$, $tRNA^{Asn}$, $tRNA^{Tyr}$ and $tRNA^{His}$ is strongly impeded. The resulting lack of those tRNAs in mitochondria significantly limits the translation within and, consequently, the function of these organelles in *T. brucei*.[26]

In the present work, we report on the crystal structure of murine QTRT1 as well as on five crystal structures of the functional murine QTRT1/QTRT2 heterodimer with and without bound queuine. In addition, we investigated the importance of QTRT2 residues Ser41 and Tyr354 on dimer

stability and determined the Michaelis-Menten parameters of murine TGT with respect to tRNA and natural as well as artificial nucleobase substrates.

RESULTS AND DISCUSSION

Determination of the Crystal Structure of Murine QTRT1 and Comparison with the Crystal Structure of Human QTRT1.

Using the naturally bound zinc ion as anomalous scatterer, we determined the crystal structure of recombinant murine QTRT1 via MAD. Diffraction quality crystals had been obtained at pH 10.5 in the presence of PEG 8000 as precipitant. The final model was refined at a resolution of 2.68 Å to an *R* factor of 18.7% and an R_{free} of 22.8% (data collection and refinement statistics are summarized in the Supporting Information, Table S1). The crystals belong to space group $P2_12_12_1$ with the asymmetric unit containing two protein molecules, which exhibit virtually identical conformations. As noticed by Johannsson et al., who had reported on the crystal structure of human QTRT1 (PDB entry 6H45),[20] the overall fold of the eukaryotic catalytic TGT subunit strongly resembles that of the protomer of the homodimeric bacterial TGT. Merely, at its C-terminus, QTRT1 possesses an additional α helix of about two and a half turns, which is not present in bacterial TGT enzymes. Residues 74 to 90, whose equivalents in bacterial TGT comprise α-helices 2a and 2b, are obviously disordered in our crystal and, thus, not defined in the electron density map (for the numbering of secondary structure elements see Figure S1). Accordingly, they are omitted from the final model. In the crystal structure of human QTRT1, this region is well defined. Yet, it does not contain any secondary structure element but forms a continuous loop.

In former work it had been shown that, in the absence of its heterodimer mate, QTRT1, the non-catalytic QTRT2 subunit forms a homodimer, which shows striking similarity to the homodimer formed by the bacterial TGT. In contrast, QTRT1 adopts a monomeric state in the absence of QTRT2.[17-19] Consistently, in the previously determined crystal structure of human QTRT1, this subunit

is clearly present as a monomer, even though the asymmetric unit contains two protein molecules.[20] At first glance, the arrangement of both protein molecules in the asymmetric unit of our murine QTRT1 crystal resembles the so-called "twisted dimer" of bacterial TGT (Figure S2). This unproductive quaternary structure, whose formation is triggered by certain inhibitors of this enzyme, is formally generated from the conventional active dimer by a ca. 130° rotation of one subunit against the other one.[27-29] However, the similarity of protein packing in the crystal structure of murine QTRT1 with the twisted dimer of bacterial TGT seems to be accidental and the corresponding protein/protein interface may represent a mere crystal contact. While the protein/protein interface of the bacterial twisted dimer virtually covers the same area as the conventional homodimer interface (> 1600 $Å^2$), the contact area between both protein molecules in the asymmetric unit of the murine QTRT1 crystal amounts to less than 800 $Å^2$. At the center of this contact, the C-termini of two equivalent α-helices, which are formed by amino acid residues Gly49 to Lys55, respectively, are in close adjacency. We refer to this secondary structure element as α helix 0 (Figure S3A). Both in the human QTRT1 and in the bacterial TGT, the corresponding residues do not form an α helix but are part of loop β1α1, which constitutes an essential component of the homodimer interface in the functional bacterial TGT. Thus, in *Z. mobilis* TGT, Lys52 within this loop is able to form a salt bridge to the side chain carboxylate of Glu339´ (the ´ indicates the dimer mate). Both Lys52 and Glu339 are virtually invariant in bacterial TGT enzymes and the mutation of one of both residues inevitably leads to an enzyme with reduced dimer stability.[16,30]

In the crystal structure of murine QTRT1, Lys55, which corresponds to Lys52 of *Z. mobilis* TGT, forms the C-terminus of α helix 0. In both QTRT1 molecules within the asymmetric unit, its side chain is only partially defined in the electron density map. Yet, it definitely does not form any salt bridge to a residue of the second QTRT1 molecule but it is encased by the side chains of Gln51, Ile57, Thr284, Arg288, Leu342, Thr346 and Thr339´ (here, the ´ indicates the second protein molecule within the asymmetric unit) without being involved in any polar interactions (Figure S3B). Facilitated by the high pH during crystallization, the side chain amine of Lys55 appears to be deprotonated. This

may allow the close proximity of Lys55 and Lys55´ in our crystal structure without a nearby negatively charged residue being required for charge compensation. Accordingly, the assembly of both protein molecules in the asymmetric unit of the murine QTRT1 crystal structure does probably not represent a homodimer which is able to form under physiological conditions.

The superposition of our murine QTRT1 structure with the crystal structure of human QTRT1 leads to almost perfect congruence of most secondary structure elements establishing the $(\beta\alpha)_8$ barrel core and the Zn^{2+} binding subdomain. Yet, significant differences between the crystal structures of both orthologues are observed as to several loop regions. As mentioned, loop β1α1 of human QTRT1 largely adopts a helical conformation in murine QTRT1 with the resulting α helix 0 establishing a crystal contact between both protein molecules within the asymmetric unit (for details see Figures S3B and S3C). This crystal contact is complemented by interactions of loop βEβF with loop αC´αD´, loop αD´αE´ and α helix E´. In addition, since both QTRT1 molecules within the asymmetric unit are related to each other by pseudo-2-fold rotational symmetry, identical interactions are formed by loop βE´βF´ with loop αCαD, loop αDαE and α helix E. Obviously caused by these interactions, loop βE(´)βF(´) experiences a significant shift compared to the equivalent loop in the crystal structure of human QTRT1 (Figure S4). Due to unfavorably close contacts, the conformation of loop βE(´)βF(´) as present in the crystal structure of murine TGT is not compatible with the conformation of loop β2(´)α2c(´) as it is observed in the crystal structure of human QTRT1. As a consequence, this section has almost completely collapsed in the structure of murine QTRT1. There is no electron density assignable to it since it is obviously disordered or scattered over multiple conformations.

A further notable difference between the crystal structures of human QTRT1 and murine QTRT1 is observed in the C-terminal halves of loop β4α4 and of loop β6α6, which form a part of the substrate binding pocket. Compared to the crystal structure of human QTRT1, this sub-pocket is substantially widened in the crystal structure of murine QTRT1 (Figure S5). Indeed, the crystal structures of the QTRT1/QTRT2 heterodimer in complex with queuine determined by us in the present study (see below) show that the conformations of these loops as observed in the structure of human

QTRT1 are the physiologically more relevant ones. The expanded substrate binding pocket as present in our structure of murine QTRT1 does obviously not support the specific recognition of the cyclopentenediol moiety of queuine. In addition, the position and orientation of Glu234 within loop β6α6 does not allow the interaction between its side chain carboxylate and the Leu230/Ser231 peptide bond which is known to be essential for the binding of the substrate´s aminomethyl group (discussed below). Therefore, the conformation of loop β6α6 as present in our structure may not facilitate the potent binding of a substrate base. Perhaps for that reason, we were, despite of considerable efforts, neither via co-crystallization nor via soaking able to obtain a crystal structure of murine QTRT1 in complex with queuine.

Determination of the Crystal Structure of the Heterodimeric Murine TGT (QTRT1/QTRT2) and Corresponding Subunit Assembly.

To investigate the architecture and functioning of the eukaryotic heterodimeric TGT, we crystallized the murine enzyme after the recombinant co-expression of the murine *QTRT1* and *QTRT2* genes and purification of the resulting heterodimer. Using the Anderson-Evans type polyoxotungstate $[TeW_6O_{24}]^{6-}$ (TEW) as additive,[31] we obtained crystals of the recombinant enzyme at pH 6.8 in the presence of PEG 1000 as precipitant. We determined the crystal structure via molecular replacement using the crystal structures of QTRT1 and QTRT2 (PDB entry 6FV5) as templates. The final model, which contains one QTRT1/QTRT2 heterodimer per asymmetric unit, was refined at 2.60 Å resolution with R and R_{free} factors amounting to 21.1% and 24.2%, respectively. Two TEW ions facilitate crystal contacts by bridging basic patches of different protein molecules. While one of the TEW ions mediates a crystal contact between two symmetry-related QTRT2 subunits, the second one interacts with the same two QTRT2 molecules and with one QTRT1 molecule (Figures S6A and S6C). Curiously, our structure displays a further polyoxotungstate cluster, which does, however, clearly differ from the TEW we had added for crystallization. The local maxima of anomalous electron density unambiguously reveal that, incompatible with the structure of TEW, it includes five instead of six tungsten ions (Figure S6D). Extensive literature search brought us to the conclusion that it might be

$[P_2W_5O_{23}]^{6-}$, which had (probably triggered by the local protein environment) spontaneously formed from TEW in the crystallization solution containing phosphate as buffer component. This Strandberg-type polyoxotungstate, whose synthesis and characterization was reported by Lin et al.,[32] excellently fits the electron density map. It is bound by two symmetry-related QTRT1 subunits with its peripheral oxides forming polar interactions with a number of main chain amides and basic side chains (Figure S6B).

Since the crystals of murine TGT that we produced with the aid of TEW diffracted to moderate resolution only, we continued to perform crystallization trials while structure determination was still ongoing. Indeed, we found a further condition yielding crystals, which diffracted to a resolution of better than 2 Å. Here, crystallization took place without TEW at pH 5.9 in a solution containing $(NH_4)_2SO_4$ and Li_2SO_4 as precipitants. Again, we determined the corresponding crystal structure via molecular replacement using the crystal structures of QTRT1 and QTRT2 as templates. The final model, which also contains one QTRT1/QTRT2 heterodimer per asymmetric unit, was refined at 1.65 Å resolution resulting in R and R_{free} factors of 17.8% and 20.1%, respectively. Disregarding the absence of any polyoxotungstates, the structure is highly similar to the TEW/$[P_2W_5O_{23}]^{6-}$-containing one, but of better quality. Accordingly, the following report will refer to the structures which are based on crystals gained via the new condition in the absence of TEW, unless stated otherwise.

As expected, the subunit assembly in the QTRT1/QTRT2 heterodimer strongly resembles that in the homodimeric bacterial TGT (Figure 2). Remarkably, within the heterodimer, α-helices 2a and 2b of QTRT1, which form contacts to α-helices C and E of QTRT2, are nearly congruent with α-helices 2a and 2b of bacterial TGT. As mentioned, in the crystal structure of human QTRT1 the corresponding residues form a continuous loop, while in the structure of murine QTRT1 this segment has collapsed and is invisible in the electron density map.

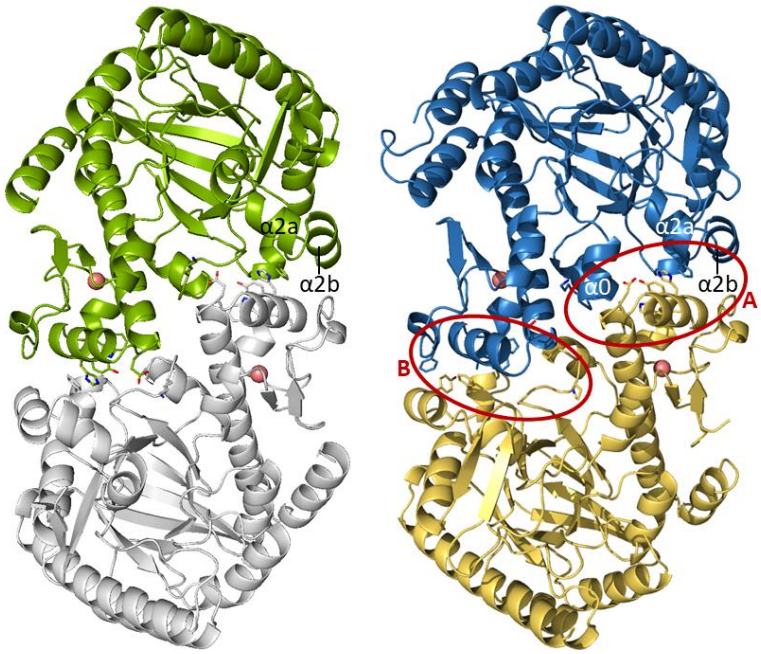

Figure 2. Ribbon representation of the *Z. mobilis* TGT homodimer (left) and the murine TGT heterodimer (right). The subunits of *Z. mobilis* TGT are colored green and gray, respectively. The QTRT1 subunit of murine TGT is shown in blue, while the QTRT2 subunit is shown in yellow. Zn^{2+} ions are depicted as spheres colored in deep salmon. The side chains of residues establishing dimer interface hot spots are shown as sticks. Hot spots A and B in the murine TGT are indicated by red ellipses.

In former studies we had shown that, in bacterial TGT, a cluster of four aromatic residues in the dimer interface is essential for dimer stability. In *Z. mobilis* TGT, this cluster consists of Trp326, Tyr330, His333 and Phe92´ (Figure 3A).[30,33] Via their hydrogen-donor functions, the side chains of Trp326, Tyr330 and His333 form hydrogen bonds (H bonds) to the main chain carbonyl oxygen atoms of Met93´, Ala49´ and Ala48´, respectively (Figure 3B). In addition, a nearby and highly conserved lysine/glutamate pair spanning both subunits (in *Z. mobilis* TGT Lys52 and Glu339´; see above) makes significant contribution to the integrity of the homodimer. Most crystal structures of *Z. mobilis* TGT with an intact dimer interface exhibit a salt bridge formed by the side chains of Lys52 and Glu339´. Yet, in a considerable number of *Z. mobilis* TGT structures, this ionic interaction is prevented by an alternative conformation of the Lys52 side chain (Figures 4A and 4B). Since the dimer mates of bacterial TGT are related to each other by an axis of 2-fold rotational symmetry, both the aromatic cluster and the lysine/glutamate pair are present twice in the dimer interface of this enzyme.

In contrast, eukaryotic TGT, which consists of two different subunits, does not possess this 2-fold symmetry. Accordingly, it contains two different versions of the corresponding arrangement of residues, which we refer to as "hot spot A" and "hot spot B". "Hot spot A" contains the mentioned

lysine/glutamate pair (Lys55 of QTRT1 and Glu372 of QTRT2) as well as an aromatic cluster which strongly resembles that of the bacterial TGT. Here, His359, Tyr363 and His366 from QTRT2 replace Trp326, Tyr330 and His333 of *Z. mobilis* TGT, while Phe95 from QTRT1 corresponds to Phe92′ of *Z. mobilis* TGT (Figure 3C). This aromatic cluster is extended by Tyr354 of the QTRT2 subunit, which forms an H bond to the main chain amide of Glu60 from QTRT1 via its phenolic hydroxyl group (Figure 3D). Tyr354 has no aromatic counterpart in *Z. mobilis* TGT. Yet, in the TGT from *Thermotoga maritima*, the only further bacterial TGT of known structure so far (PDB entry 2ASH), the corresponding position is occupied by Tyr302 forming an equivalent H bond. In contrast, His359, Tyr363 and His366 from QTRT2 are not able to form H bonds to the main chain carbonyl groups of Met96, Ala52 and Gln51 of QTRT1 (which, in primary structure, correspond to Met93, Ala49 and Ala48 of *Z. mobilis* TGT). Rather, these contacts are replaced by several water-mediated polar interactions between the dimer mates (Figure 3D). This is due to the fact that, in the crystal structure of the murine QTRT1/QTRT2 heterodimer, residues Gly49 to Lys55 of QTRT1, whose counterparts in bacterial TGT are part of loop β1α1, adopt the same helical conformation as observed in the crystal structure of murine QTRT1. Via the main chain carbonyl oxygen atoms of Thr53 and Met54, the resulting α helix 0 forms H bonds to the main chain amides of Leu374 and Leu373 of QTRT2, which constitute the N-terminus of α helix F of this subunit (Figure 4C).

This interface architecture leads to a positioning of Lys55 of QTRT1 which excludes the formation of a salt bridge to the side chain carboxylate of Glu372 of QTRT2. Indeed, the Lys55 side chain, which is well-defined in the electron density map, is present in a similar conformation as in the crystal structure of murine QTRT1. However, within the heterodimer it is more solvent exposed with its ammonium group forming an H bond (2.8 Å) to a nearby water molecule (Figure S3D). It must be noted that, in *Z. mobilis* TGT, Lys52 does not only contribute to dimer stability but is involved in tRNA binding as well. The crystal structure of *Z. mobilis* TGT in complex with an RNA molecule reveals a cation-π interaction formed by the side chain ammonium of Lys52 and uracil-35 of the tRNA substrate.[15] However, this interaction will only form if the Lys52 side chain is present in a conformation

allowing a salt bridge to the side chain carboxylate of Glu339´. Accordingly, the positioning of Lys55 of QTRT1 in the crystal structure of the murine QTRT1/QTRT2 heterodimer clearly precludes such a cation-π interaction. Therefore, it seems unavoidable that the binding of the tRNA substrate entails significant conformational change in this region.

Notably, while this manuscript was in preparation, the crystal structure of the human TGT enzyme in complex with an RNA oligonucleotide mimicking the anticodon stem loop of a $tRNA^{Tyr}$ was published.[34] Here, residues 49 to 55 of QTRT1 do not form α helix 0 but are part of loop β1α1, which is present in a conformation that strongly resembles that of its counterpart in bacterial TGT. This allows the above mentioned subunit-bridging H bonds of His359, Tyr363 and His366 of QTRT2 to the main chain carbonyl groups of Met96, Ala52 and Gln51 of QTRT1, which are not able to form in the crystal structure of murine TGT. Furthermore, Lys55 of QTRT1 adopts a conformation similar to that of Lys52 of *Z. mobilis* TGT in complex with an RNA molecule and it forms a cation-π interaction with uracil-35.

"Hot spot B" in the crystal structure of murine TGT does not contain a lysine/glutamate pair analogous to Lys52´ and Glu339 of *Z. mobilis* TGT. The corresponding positions are occupied by Pro43 of QTRT2 and Asn338 of QTRT1, which are unable to form an ionic interaction (Figure 4D). Furthermore, the aromatic cluster of "hot spot B" lacks an aromatic residue equivalent to His333 of *Z. mobilis* TGT (Figures 3E and 3F). Rather, this position is occupied by Ala332 of QTRT1. In contrast, there are counterparts to Trp326, Tyr330 and Phe92´ of *Z. mobilis* TGT, namely His325 and Phe329 of QTRT1 as well as Phe84 of QTRT2. Loop β1α1 of QTRT2 takes a course which is highly similar to that observed in the crystal structures of bacterial TGT with intact dimer interface. Yet, no H bond can be formed between any main chain carbonyl oxygen atoms within this loop and aromatic residues of the cluster. As mentioned, there is no counterpart of His333 of *Z. mobilis* TGT and the side chain of Phe329 of QTRT1 is devoid of any hydrogen donor function. His325 of QTRT1, however, is in the position to form an H bond to the main chain carbonyl oxygen of Ile85 of QTRT2 analogous to the H bond formed by Trp326 and Met93´ in *Z. mobilis* TGT. The absence of a counterpart of His333 in "hot spot

B" may be partially compensated by two additional aromatic residues, Tyr77 of QTRT2 and Phe310 of QTRT1, at the opposing end of the cluster. The phenyl moiety of Tyr77 of QTRT2 implements edge-to-face π-π interactions both with the phenyl group of Phe84 of the same subunit and with the phenyl group of Phe310 of QTRT1 (Figure 3G). In addition, α helix F of QTRT1 contributes another two aromatic residues to the cluster, namely His343 and His344. The imidazole of the latter histidine is involved in edge-to-face π-π interactions both with the imidazole of His325 and with the imidazole of His343 from QTRT1.

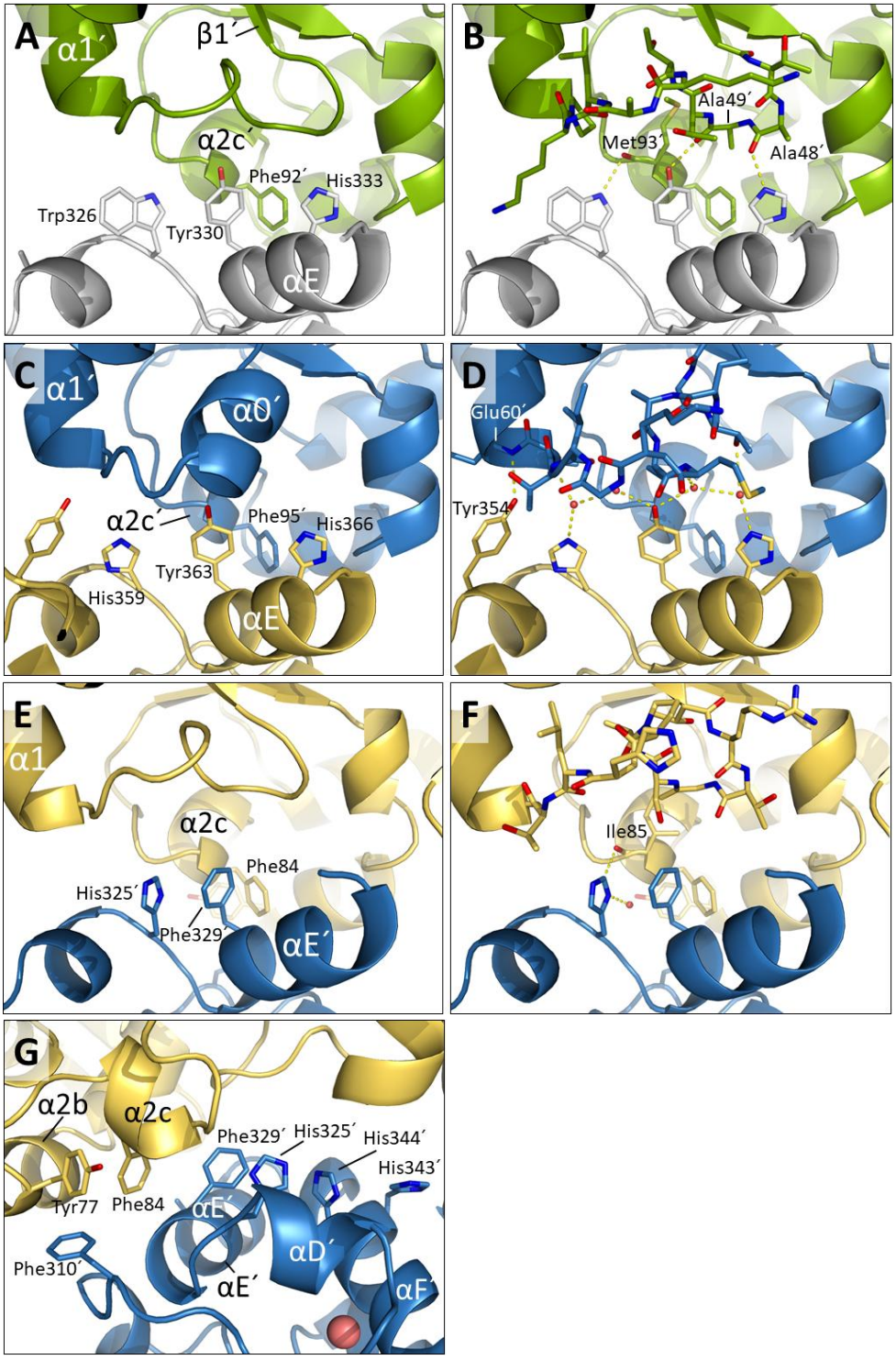

Figure 3. The aromatic cluster in the dimer interfaces of the bacterial and of the murine TGT. (A) The aromatic cluster of the bacterial TGT dimer interface (PDB entry 1P0D). The protein is shown in ribbon representation with one subunit colored green, the other one grey. The side chains of residues forming the cluster are shown as sticks. Residues and secondary structure elements of the green-colored subunit are indicated by a ´. (B) The same as (A) but residues forming loop β1´α1´ as well as Met93´ are shown as sticks. H bonds are indicated by dotted lines. (C) The aromatic cluster in "hot spot A" of the murine QTRT1 (blue) / QTRT2 (yellow) interface with the side chains of residues forming the cluster shown as sticks. Residues and secondary structure elements of QTRT1 are indicated by a ´. (D) The same as C) but residues connecting β strand 1´ and α helix 1´ (including α helix 0´) as well as Glu60´ are shown as sticks. Water molecules are depicted as red spheres. (E) The aromatic cluster in "hot spot B" of the murine QTRT1/QTRT2 interface with the side chains of residues forming the cluster being shown as sticks. (F) The same as (E) but residues forming loop β1α1 as well as Ile85 are shown as sticks too. His325´ may form a weak H bond (3.3 Å) to the main chain carbonyl oxygen atom of Ile85. Yet, a water molecule is in H bond distance to the His325´ imidazole as well (3.0 Å). Since both putative H bonds exclude each other, the orientation of the His325´ imidazole remains unclear. (G) The aromatic cluster in "hot spot B" from a different point of view visualizing the edge-to-face π-π interactions of the Tyr77 aromatic side chain with those of Phe84 and Phe310´ as well as the edge-to-face π-π interactions of the His344´ imidazole with the imidazole rings of His325´ and His343´. The sphere colored in deep salmon represents a Zn^{2+} ion.

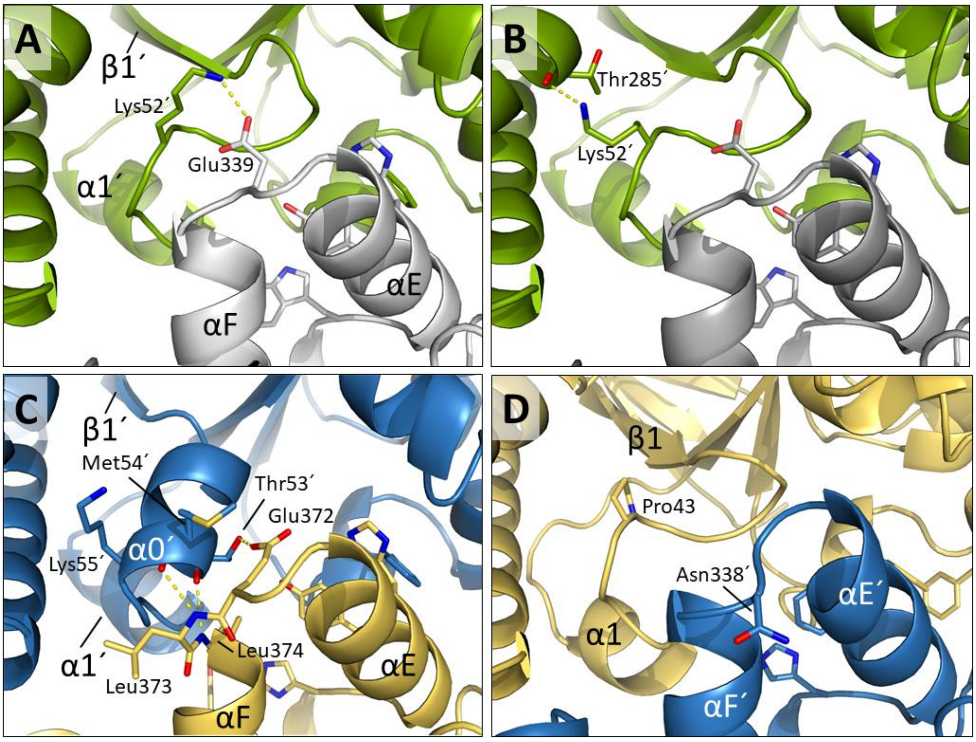

Figure 4. Subunit spanning lysine/glutamate pair in TGT enzymes. Color coding and labeling corresponds to that in Figure 3. (A) In about two thirds of the crystal structures of *Z. mobilis* TGT with intact dimer interface, Lys52´ and Glu339 form a salt bridge (here, PDB entry 2Z7K). In addition to the side chains of Lys52´ and Glu339, those of the aromatic cluster are shown as sticks with the latter ones not being labeled. (B) In about one third of the *Z. mobilis* TGT crystal structures with undisturbed dimer interface the Lys52´ side chain is present in an alternative conformation resulting in a charge-assisted H bond to the main chain carbonyl oxygen of Thr285´, which is shown in stick representation (the detail is from PDB entry 1PUD). (C) In "hot spot A" of the murine TGT the formation of α helix 0 in QTRT1 does not allow Lys55 of QTRT1 to form a salt bridge with Glu372 of QTRT2. (D) In "hot spot B", the lysine/glutamate pair is replaced by a proline (Pro43 of QTRT2) and by an asparagine (Asn338 of QTRT1) excluding the formation of a salt bridge.

The Significance of QTRT2 Residues Ser41 and Tyr354 for Dimer Stability.

As mentioned, the aromatic cluster within “hot spot A” of the QTRT1/QTRT2 heterodimer interface closely resembles the aromatic cluster within the homodimer interface of *Z. mobilis* TGT. In former work, we have extensively studied the roles which the counterparts of QTRT2 residues His359, Tyr363 and His366 play for the stability of the dimer interface of bacterial TGT.[30,33,35] There is, however, no evidence about the importance of QTRT2 residue Tyr354 for dimer stability since a corresponding aromatic residue does not exist in *Z. mobilis* TGT. The crystal structure of murine QTRT2, published by us in 2018,[19] reveals that this residue not only seems to be of relevance for the stability of the TGT heterodimer but also for the stability of the QTRT2 homodimer. Here, it forms a subunit-bridging H bond to the main chain amide of Gln48´. In addition, the QTRT2 homodimer appears to be stabilized by an H bond formed between the side chain hydroxyl group of Ser41 and the phenolic

hydroxyl group of Tyr363´ (Figure S7). In contrast, in the crystal structure of the TGT heterodimer, no polar interaction of Ser41 with any residue of QTRT1 is observed. To investigate the significance of the hydroxyl groups of Ser41 and Tyr354 for hetero- as well as for homodimer stability we created mutated variants of QTRT2 in which these residues were changed to alanine and phenylalanine, respectively. Then, we analyzed the impact of the respective mutations on dimer stability via native mass spectrometry coupled to size exclusion chromatography (SEC-nMS) using separately produced and purified QTRT1 and QTRT2 subunits.

As shown before,[17-19] QTRT2 is mainly present as a homodimer in the absence of QTRT1, while QTRT1 is almost exclusively present as a monomer in the absence of QTRT2. Since proteins with greater hydrodynamic volumes will elute faster from the SEC column, homodimeric QTRT2 and mutated variants thereof exhibit lower retention times (3.05 min) in comparison with monomeric QTRT1 (3.48 min) (Figure 5A).

SEC results are supported and complemented by online nMS (Figure 5B). While the observed mass for QTRT1 was 44301 ± 1 Da, the masses of wild type QTRT2, QTRT2(Ser41Ala), QTRT2(Tyr354Phe), and QTRT2(Ser41Ala/Tyr354Phe) were 94452 ± 1 Da, 94421 ± 1 Da, 94425 ± 1 Da, and 94394 ± 3 Da, respectively, being in good agreement with the masses of the corresponding homodimer species. However, a less intense distribution that corresponds to the monomeric structure of QTRT2 variants is also observed in the mass spectra. Since no signal corresponding to the monomeric structure of QTRT2 is observed in the SEC profile it can be concluded that QTRT2 homodimer slightly dissociates within the interface of the mass spectrometer during the ESI process. Remarkably, the point mutations introduced into QTRT2 lead to increased MS intensities of the monomeric structures (Figure 5B). While, in the mass spectrum of QTRT2(Ser41Ala), the monomeric portion is marginally increased compared with wild type QTRT2 (in both cases lower than 25%), it is strongly elevated in the mass spectra of QTRT2(Tyr354Phe) and QTRT2(Ser41Ala/Tyr354Phe) (around 35% of relative intensity). Accordingly, our results indicate a pronounced stabilizing effect of the H bond formed between the phenolic hydroxyl group of Tyr354 and the main chain amide of Gln48´ for

QTRT2 homodimer integrity. The disruption of this noncovalent interaction impairs the stability of the homodimer interface, thus favoring the dissociation of the dimer when proteins are transferred into the gas phase (Figure 5B).

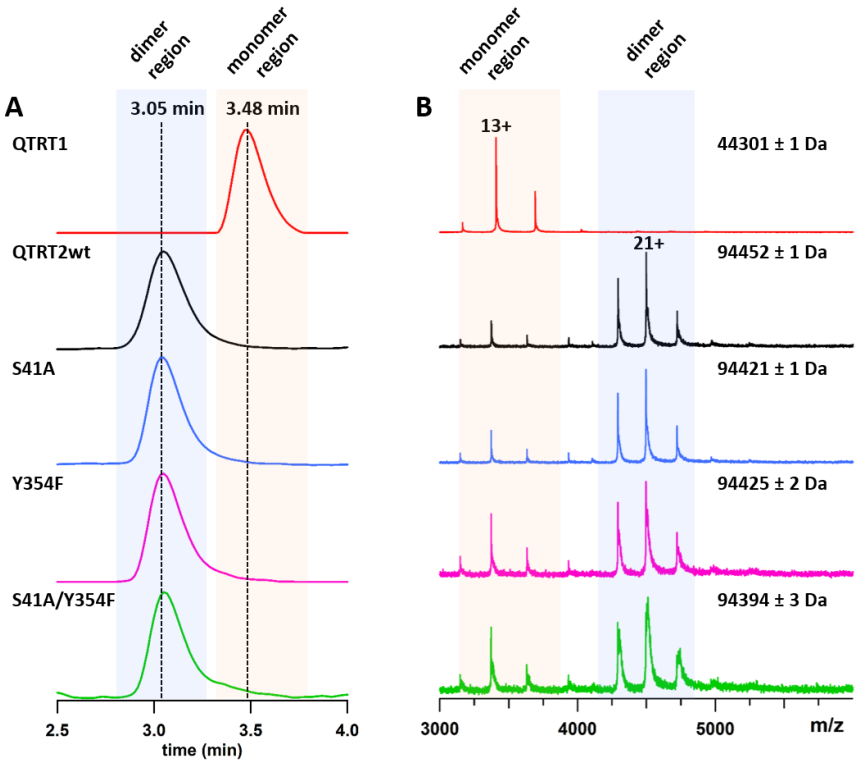

Figure 5. SEC-nMS analysis of QTRT1, QTRT2, and different mutated QTRT2 variants. (A) SEC profiles of proteins. (B) nMS signal corresponding to the chromatographic peak of each individual compound. The plots were created using Igor Pro version
6.0.5.0 (WaveMetrics Inc, Lake Oswego, Oregon, USA).

The same experimental set-up was used to study the equimolar mixtures of QTRT1 and different QTRT2 variants. Overall, two different signals were observed on the SEC profile at 3.05 min and 3.48 min, the latter corresponding to the unbound QTRT1 monomer (Figure 6A). While the Ser41Ala mutation in QTRT2 does not significantly affect the relative intensity of QTRT1 monomer, the proportion of unbound QTRT1 decreases when QTRT2 variants bearing the Tyr354Phe mutation are involved in the equimolar mixture (Figure 6A). The nMS signal associated to the main SEC peak at 3.05 min clearly evidences the coexistence of homodimeric and heterodimeric species for all the equimolar mixtures (Figure 6B), although the most predominant signal corresponds to the heterodimeric form of the proteins for all the different QTRT2 variants. These mass spectra clearly show that QTRT1/QTRT2 heterodimer formation is favored in the case of QTRT2(Tyr354Phe), and

QTRT2(Ser41Ala/Tyr354Phe). Overall, the relative intensity of QTRT1/QTRT2 heterodimer is in good agreement with the relative intensity of the unbound QTRT1 monomer for all the different mixtures (Figure 6C), i.e., the lowest relative intensity of unbound QTRT1 monomer corresponds with the highest relative intensity of the heterodimer complex. Thereby, QTRT2(Tyr354Phe) and QTRT2(Ser41Ala/Tyr354Phe) exhibit the lowest amounts of unbound QTRT1 monomer along with the highest heterodimer/homodimer ratio, suggesting that the Tyr354Phe mutation promotes the formation of the QTRT1/QTRT2 heterodimer. Due to the loss of the H bond formed between the phenolic hydroxyl group of Tyr354 in QTRT2 and the main chain amide of Glu60 in QTRT1, the Tyr354Phe mutation is expected to have a destabilizing effect on the heterodimer. Yet, due to 2-fold rotational symmetry, an equivalent H bond formed by the phenolic hydroxyl group of Tyr354 and the main chain amide of Gln48´ is present twice in the interface of the QTRT2 homodimer. Therefore, the impact on dimer stability caused by the Tyr354Phe mutation is likely to be much more pronounced in the QTRT2 homodimer than in the QTRT1/QTRT2 heterodimer. As a result, equilibrium is shifted from the heavily destabilized QTRT2 homodimer towards the QTRT1/QTRT2 heterodimer whose stability is considerably less compromised by the Tyr354Phe mutation.

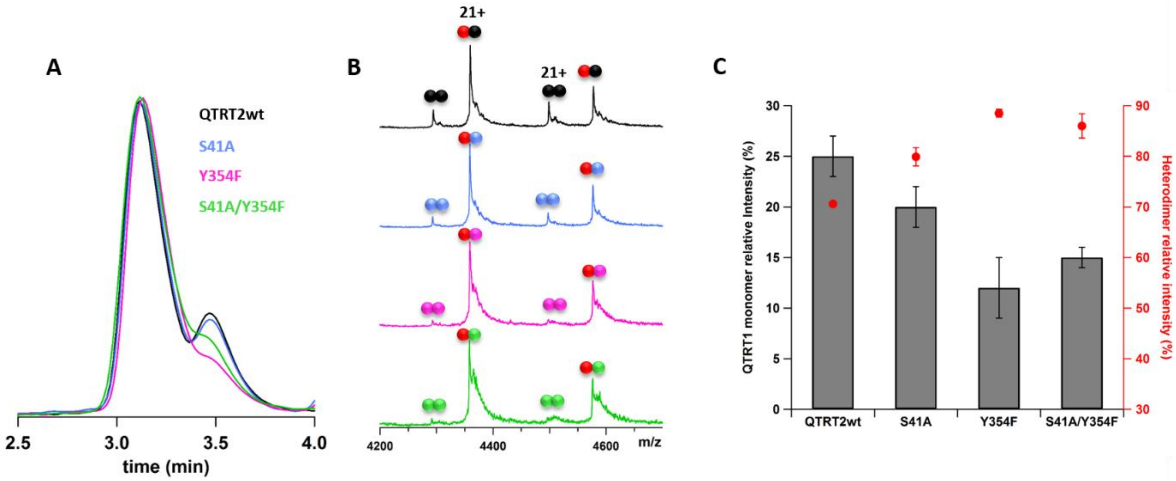

Figure 6. SEC-nMS experiments of equimolar mixtures of QTRT1 and QTRT2 variants. (A) Superimposed SEC profiles of equimolar mixtures of QTRT1 with wild type QTRT2 (black line), QTRT2(Ser41Ala) (blue line), QTRT2(Tyr354Phe) (pink line), and QTRT2(Ser41Ala/Tyr354Phe) (green line). (B) nMS spectra of individual mixtures showing the presence of homodimer and heterodimer populations. (C) Correlation between the relative intensities of unbound QTRT1 monomer and the heterodimer relative intensities upon mixture of QTRT1 with each individual QTRT2 variant. The relative quantification of all species were performed in triplicate under strictly identical experimental and instrumental conditions. The plots were created using Igor Pro version 6.0.5.0 (WaveMetrics Inc, Lake Oswego, Oregon, USA).

To figure out if the studied QTRT2 mutations affect the enzymatic activity of murine TGT, we determined k_{cat} as well as $K_m(tRNA^{Tyr})$ of murine TGT variants reconstituted from separately produced QTRT1 and (mutated) QTRT2. Kinetic measurements were done via a well-established assay monitoring the incorporation of radiolabeled guanine into $tRNA^{Tyr}$. $K_m(tRNA^{Tyr})$ turned out virtually identical for all analyzed TGT variants revealing that none of the introduced mutations affects tRNA binding (Table 1). In contrast, compared to wild type TGT, we measured slightly reduced turnover numbers (k_{cat}) for TGT enzymes containing any of the mutated QTRT2 variants. While marginal (< 2-fold) reduction of k_{cat} is observed for TGT containing QTRT2(Tyr354Phe), k_{cat} is decreased by a factor of 2.5 for TGT containing QTRT2(Ser41Ala). Consistently, the lowest turnover number was determined for TGT containing doubly mutated QTRT2(Ser41Ala/Tyr354Phe) where k_{cat} is about 3.5-fold reduced. A similar phenomenon has been repeatedly observed in bacterial TGT. In most cases, the mutation of a residue involved in establishing the dimer interface does not interfere with tRNA binding but slightly reduces k_{cat}.[30,33,35]

Table 1. Kinetic parameters of murine TGT (obtained after the reconstitution of separately produced and purified QTRT1 and QTRT2 variants).

	$K_m(tRNA^{Tyr})$ [µmol L^{-1}]	k_{cat} [10^{-3} s^{-1}]
QTRT1/QTRT2(wild type)	0.59 ± 0.08	4.9 ± 0.2
QTRT1/QTRT2(Ser41Ala)	0.45 ± 0.05	1.9 ± 0.1
QTRT1/QTRT2(Tyr354Phe)	0.37 ± 0.04	3.0 ± 0.1
QTRT1/QTRT2(Ser41Ala/Tyr354Phe)	0.47 ± 0.04	1.3 ± 0.1

For progress curves and resulting Michaelis-Menten plots, see Figure S8.

Kinetic Parameters and Substrate Base Specificity of Murine TGT.

Chen et al. had reported that, in an attempt to reconstitute the recombinant human TGT enzyme from individually prepared QTRT1 and QTRT2 subunits, they had observed very low levels of enzyme activity.[18] Only after the recombinant co-expression of the human *QTRT1* and *QTRT2* genes and purification of the resulting heterodimer they were able to gain highly active enzyme suitable for the determination of Michaelis-Menten parameters. In contrast, for the murine enzyme whose sub-

units had been produced separately and combined in a molar ratio of 1 : 1, we realized activity which is only slightly lower than that generally observed for the bacterial enzyme [K_m(tRNA^{Tyr}) of the *Z. mobilis* TGT was determined to 0.8 ± 0.1 µmol L^{-1} and k_{cat} to (9.0 ± 0.3) · 10^{-3} s^{-1} by Nguyen et al.].[35] Nonetheless, to figure out if the mode of preparation has an influence on the enzymatic activity of the recombinant murine TGT too, we re-determined Michaelis-Menten parameters regarding tRNA^{Tyr} and guanine employing the enzyme we had used for crystallization. As mentioned, this preparation had been obtained via the dual recombinant expression of the *QTRT1* and *QTRT2* genes followed by the purification of the heterodimeric protein immediately generated in the bacterial cell. The activity of this enzyme turned out to be marginally higher than the activity of the enzyme gained after the separate expression of the *QTRT1* and *QTRT2* genes. Indeed, we determined k_{cat}(tRNA^{Tyr}/guanine) as well as K_m(tRNA^{Tyr}) and K_m(guanine) values which are virtually identical with those previously measured for the recombinant human enzyme by Chen et al.[18] (see Table 2).

In addition, we determined k_{cat} values for the naturally occurring TGT substrates queuine, preQ$_1$ base, and preQ$_0$ base, as well as for the artificial substrates “dihydroqueuine”, NPPDAG, and 8-azaguanine by recording progress curves at saturating concentrations of these compounds (for structural formulae see Figure 1). However, disregarding guanine, radiolabeled bases acting as substrates of TGT are either commercially not available or if they are, at enormously high costs. Accordingly, we determined k_{cat} values for these substrates via a “washout assay”, which was essentially first described by Hoops et al..[36] It relies on monitoring the decrease in radioactivity of tRNA^{Tyr}, enzymatically pre-labeled with [8-^{3}H]-guanine in position 34, due to the incorporation of the respective “cold” substrate base.

This method implies high initial radioactive signals whose time-dependent decrease will be very small at low substrate concentrations as they are partially necessary for the determination of K_m values. Accordingly, corresponding progress curves will be afflicted with low signal to noise ratio and, therefore, be little accurate. For that reason, we did not use the “washout assay” to measure K_m values for the mentioned substrate bases. Instead, we used the conventional assay applying tRNA^{Tyr} and

[8-^{3}H]-guanine to figure out the affinities of these substrates to the enzyme. Thereby, we used them as competitive inhibitors with respect to [8-^{3}H]-guanine and determined K_i values as substitutes of K_m. Clearly, in contrast to real competitive inhibitors, substrate bases are inserted into tRNA, which results in the decrease of their concentration. In addition, if the insertion of the respective base into tRNA occurs irreversibly, substrate tRNA^{Tyr} concentration will decrease as well. Yet, during the measurement of initial velocities, this time-dependent drop in concentration is deemed negligible regarding the error range involved in such kind of assay. To verify the usefulness of this approach, we determined k_{cat} as well as K_i for "cold" guanine. Indeed, k_{cat}(guanine) obtained by means of the washout assay turned out to be identical with k_{cat}([8-^{3}H]-guanine) determined via the conventional assay. In addition, we measured a K_i value for this base which does, within error range, hardly differ from K_m([8-^{3}H]-guanine) (Table 2).

Table 2. Kinetic parameters of murine TGT (obtained after co-expression of the *QTRT1* and the *QTRT2* genes) regarding tRNA^{Tyr} and various substrate bases.

	K_m [µmol L^{-1}]	k_{cat} [10^{-3} s^{-1}]
tRNA^{Tyr}	0.44 ± 0.08 (0.34 ± 0.04)	6.5 ± 0.3 (5.6 ± 0.1)
[8-^{3}H]-guanine	0.40 ± 0.03 (0.41 ± 0.03)	6.0 ± 0.1 (5.9 ± 0.1)
	K_i [µmol L^{-1}]	k_{cat} [10^{-3} s^{-1}]
guanine	0.68 ± 0.07	6.3 ± 0.5
queuine	0.33 ± 0.02	12.1 ± 1.0
preQ$_1$ base	17.0 ± 1.0	7.8 ± 0.4
preQ$_0$ base	0.14 ± 0.07	4.9 ± 0.5
dihydroqueuine	8.6 ± 0.4	6.0 ± 0.7
NPPDAG	10.0 ± 0.3	5.6 ± 0.5
8-azaguanine	0.99 ± 0.04	6.3 ± 0.6

For progress curves and resulting Michaelis-Menten plots for tRNA^{Tyr} and [8-^{3}H]-guanine see Figure S9; progress curves obtained from the "washout assay" (determination of k_{cat} for "cold" substrate bases) are shown in Figure S10, while Figure S11 shows progress curves and resulting Dixon plots for the determination of K_i values. K_m and k_{cat} values in brackets were determined for the recombinant human enzyme by Chen et al.[18]

Queuine, the physiological substrate of eukaryotic TGT, is recognized by the enzyme with an affinity nearly equaling that of guanine [K_i(queuine) ≈0.3 µmol L^{-1}]. Yet, using queuine as substrate

we measured a turnover number (k_{cat} ≈12 · 10^{-3} s^{-1}) twice as high as that measured with guanine (k_{cat} ≈6 · 10^{-3} s^{-1}) suggesting that queuine may be inserted into tRNA at somewhat higher rate. The $preQ_1$ base, which constitutes the physiological substrate of bacterial but not of eukaryotic TGT, is inserted into tRNA by the murine TGT with similar turnover as guanine [$k_{cat}(preQ_1)$ ≈8 · 10^{-3} s^{-1}]. However, its affinity to this enzyme is, compared to that of guanine and queuine, strongly decreased [$K_i(preQ_1)$ ≈17 µmol L^{-1}]. This fact, which was observed by Chen et al. for the human TGT as well,[18] is of physiological importance since the insertion of the $preQ_1$ base into tRNA is irreversible. Thus, it has to be avoided, since eukaryotes do not possess the enzymes required for the conversion of the $preQ_1$ nucleoside to queuosine. Okada et al. reported that a single cell of *Escherichia coli*, a representative of the gut microbiome, which constitutes a major source of TGT substrates in animals and human, contains about one thousand molecules of free $preQ_1$ base. In contrast, its immediate biosynthetic precursor, the $preQ_0$ base (7-nitrilo-7-deazaguanine), which constitutes a substrate of TGT too, is hardly detectable in *E. coli*.[37] Furthermore, the insertion of the $preQ_0$ base into tRNA is reversible, which is why no harm will be done if it is efficiently recognized as a substrate by the eukaryotic TGT. Indeed, the K_i of 0.14 µmol L^{-1} measured for this base is even slightly lower than $K_{m/i}$(guanine) and K_i(queuine) with k_{cat} amounting to ≈5 · 10^{-3} s^{-1}, a value similar to that measured for guanine and the $preQ_1$ base.

Already in 1984, Farkas et al., who had partially purified the TGT from rabbit reticulocytes, noted that “dihydroqueuine”, in which the double bond in the cyclopentenediol moiety of queuine is saturated, represents a considerably poorer substrate of this enzyme than queuine.[38] Our data show that dihydroqueuine is inserted into tRNA with a similar rate as guanine and $preQ_1$ base. Yet, its affinity to the enzyme is, compared with that of queuine, about 30-fold reduced suggesting a significant role of the double bond in the five-membered ring of queuine in recognition by the TGT enzyme. A further artificial substrate of eukaryotic TGT of note is the synthetic 7-deazaguanine derivative NPPDAG. When incorporated into tRNA, it is able to induce remarkable recovery of clinical symptoms in experimental autoimmune encephalomyelitis, a mouse model of multiple sclerosis.[23] As shown in Table 2, both k_{cat}(NPPDAG) and K_i(NPPDAG) strongly resemble the corresponding values determined

for dihydroqueuine. Ultimately, we analyzed 8-azaguanine, whose TGT-dependent insertion into tRNA occurs, like that of guanine, reversibly.[38] The affinity of this base to the enzyme (K_i ≈1 µmol L^{-1}) is similar to that of guanine and it is inserted into tRNA at identical rate.

The Active Center of Murine TGT.

To deepen our understanding of substrate base binding and of catalysis, we investigated the active center of murine TGT at a structural level. In our crystal structure of murine TGT obtained in the absence of TEW the guanine-34/queuine binding pocket of QTRT1 is occupied by a citrate molecule, which served as buffer component during crystallization (Figure S12A). The bound citrate forms numerous polar interactions with residues known to be involved in substrate binding. One of its carboxyl groups forms H bonds to the side chain amide of Gln202 and to the side chain carboxyl of Asp159. The latter interaction suggests that this carboxyl of the bound citrate is protonated, mimicking the carbonyl oxygen at position 6 and the NH at position 1 of a bound substrate base (Figure 7A). The hydroxyl group of the citrate forms H bonds to the main chain amide of Gly229 and to a well-defined water molecule, while the carboxyl group attached to the same carbon atom is solvent-exposed and not involved in any visible interactions. The third carboxyl group of the bound citrate forms H bonds both to the side chain hydroxyl and to the main chain amide of Ser231. The latter interaction requires the amide of the Leu230/Ser231 peptide bond to be exposed to the substrate binding pocket, while its carbonyl oxygen forms an H bond to the protonated side chain carboxyl group of Glu234. Not only in the QTRT1 subunits of eukaryotic TGTs but also in bacterial TGTs, Glu234 is strictly conserved since it plays an essential role in the adaptation of the binding pocket to different substrate bases. From a study on the bacterial TGT it is known that the observed conformation of the Leu230/Ser231 peptide bond, which is stabilized by the protonated Glu234, is required for the accommodation of guanine-34.[39]

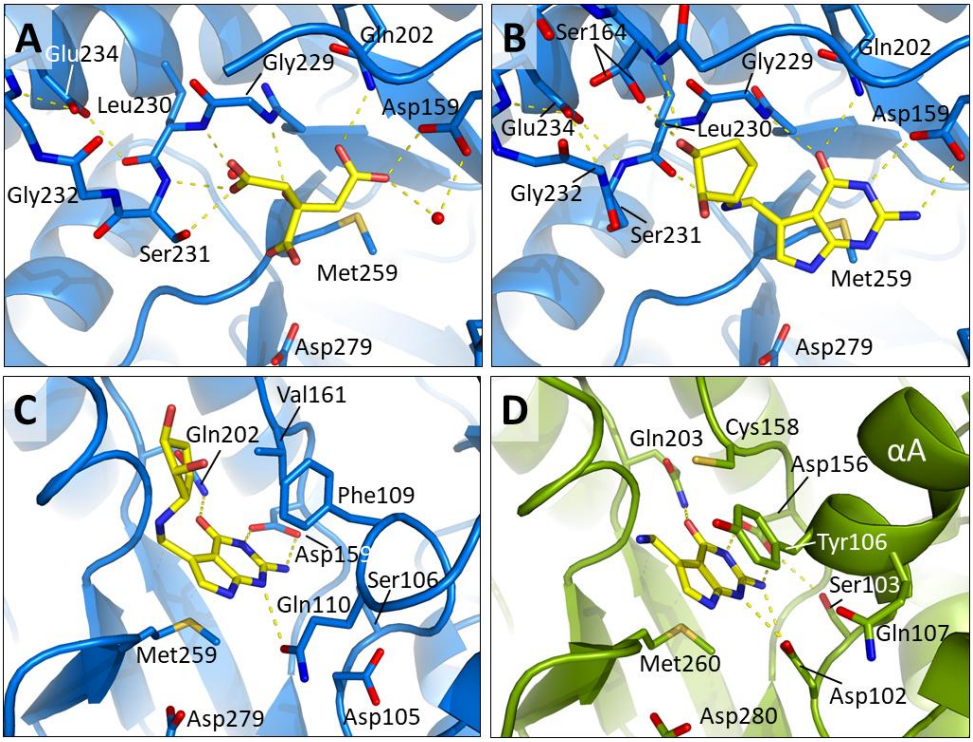

Figure 7. The substrate base binding pocket in murine QTRT1 (blue) compared with that of *Z. mobilis* TGT (green). H bonds are indicated by dotted lines. (A) The guanine/queuine binding pocket in murine QTRT1 occupied by citrate (shown in stick representation; carbon atoms yellow). Two water molecules forming H bonds to the bound citrate are shown as red spheres. Loop β6α6 as well as the side chains of residues known to be involved in the binding of substrate bases or in catalysis are shown in stick representation. The remainder of the protein within this detail is shown in ribbon representation. (B) The same view of the guanine/queuine binding pocket in murine QTRT1 as in (A) but with queuine bound. (C) A different view of the queuine-bound guanine/queuine binding pocket of murine QTRT1. The side chains of residues known to be involved in the binding of substrate bases or in catalysis are shown in stick representation. (D) The guanine/preQ$_1$ binding pocket of the *Z. mobilis* TGT with bound preQ$_1$ base (PDB entry 1P0E) shown from a view equivalent to that in (C).

To decipher the binding mode of queuine in the active center of eukaryotic TGT we determined the crystal structure of the murine enzyme in complex with this substrate base. However, co-crystallization of the enzyme with queuine had failed at pH 5.9 using $(NH_4)_2SO_4$ and Li_2SO_4 as precipitants, since, under this condition, the presence of queuine turned out to prevent crystallization. Obviously, the binding of the buffer component, citrate, into the binding pocket of murine TGT is prerequisite for the formation of well-diffracting crystals but it is impeded by the potent substrate base. We only obtained high-quality crystals of the desired complex via soaking queuine into pre-existing TGT crystals that had been transferred into a solution in which citrate was replaced by 2-(*N*-morpholino)ethanesulfonic acid (MES) (with the latter not being able to replace citrate during crystallization). Although this procedure slightly affected diffraction quality, we were able to determine the crystal structure of murine TGT in complex with queuine at a resolution of 2.1 Å with the bound queuine molecule being well-defined in the electron density map (Figure S12B). In contrast, no elec-

tron density assignable to citrate or to any other ligand is detectable in the structure of a crystal that had been transferred into MES solution without subsequent soaking of queuine. As expected, the 7-deazaguanine scaffold of queuine bound to murine TGT is nearly identically placed in the binding pocket as that of $preQ_1$ base in the binding pocket of bacterial TGT. Thus, its 1-NH group and its 2-amino group form H bonds to the side chain carboxylate of Asp159 while the carbonyl oxygen at position 6 forms H bonds to the side chain amide of Gln202 and to the main chain amide of Gly229 (Figures 7B and 7C). The aromatic scaffold is placed between the side chains of Met259 and Phe109 with Met259 being virtually congruent with the corresponding Met260 in *Z. mobilis* TGT (Figure 7D). In contrast, the Cα atom of Phe109 is, compared with that of the equivalent Tyr106 in *Z. mobilis* TGT, shifted away from the base by about 2.3 Å. This allows the rotation of the phenyl group of Phe109 which, as a result, does not form a face-to-face but an edge-to-face π-π interaction with the 7-deazaguanine scaffold. The shift of Phe109 is a consequence of the conformation, residues 108 to 114 adopt in the crystal structure of murine TGT. While these residues constitute α helix A in the crystal structures of both human and murine QTRT1 (the same applies to the equivalent residues of *Z. mobilis* TGT), they form a loop in the crystal structure of murine TGT.

In the crystal structure of *Z. mobilis* TGT in complex with the $preQ_1$ base, obtained after co-crystallization at pH 5.5 (PDB ID 1P0E), the side chain carboxylate of Asp102 forms a salt bridge to the obviously protonated N3 and to the 2-amino group of the substrate base[40] (Figure 7D). In the crystal structure of murine TGT in complex with queuine an equivalent salt bridge is not observed. It is sterically prevented by the placement of Gln110, whose side chain is pushed between the substrate base and Asp105 (corresponding to Asp102 of *Z. mobilis* TGT) (Figure 7C). This placement of Gln110 is a further consequence of the mentioned loop conformation of residues 108 to 114. Since this loop would produce a clash with the uridine-35 nucleotide of a bound tRNA substrate, it may constitute a crystallographic artefact. At least upon tRNA binding it will likely rearrange to α helix A. In our crystal structure of murine TGT, the side chain carboxylate of Asp105 is oriented away from the substrate

base forming an H bond to the main chain amide of Thr74. Notably, in the crystal structure of *Z. mobilis* TGT in its apo-form (PDB ID 1PUD), Asp102 is present in an equivalent conformation.

The exchange of citrate by queuine in the binding pocket causes a flip of the above-mentioned Leu230/Ser231 peptide bond. Now, its carbonyl oxygen faces the binding pocket enabling the formation of an H bond to the secondary ammonium of the substrate base (Figure 7B). This peptide bond conformation is stabilized by the side chain carboxyl group of Glu234 too. Yet, concomitant with the peptide flip, the latter has been deprotonated allowing for an H bond to the amide of the peptide bond, which is now directed away from the binding pocket. An analogous phenomenon is observed in bacterial TGT. Here, the binding of the $preQ_1$ base inevitably leads to the deprotonation of Glu235 (*Z. mobilis* TGT numbering) which, thereupon, forms an H bond to the amide of the Leu231/Ala232 peptide bond. In this conformation its carbonyl oxygen is oriented into the binding pocket where it forms an H bond to the protonated aminomethyl group of the $preQ_1$ base.[39] In the absence of a bound substrate base, the conformation of the Leu231/Ala232 peptide bond from *Z. mobilis* TGT depends on the pH adjusted during crystallization. If crystallized at pH 5.5, Glu235 will be protonated and will form an H bond with the carbonyl oxygen of this peptide bond. Consequently, the amide of the peptide bond will face the binding pocket. If, however, crystallization takes place at pH 8.5, Glu235 will be deprotonated. As a result, it forms an H bond with the amide of the Leu231/Ala232 peptide bond, whose carbonyl oxygen atom is directed into the binding pocket. In the crystal structure of murine apo-TGT, which was gained by transferring a citrate-bound crystal into MES containing buffer (pH 5.9), the Leu230/Ser231 peptide bond adopts both possible conformations (occupancies refined to 58% and 42%, respectively). Hence, at pH 5.9, Glu234 of QTRT1 is obviously present both in its protonated and deprotonated form in comparable quantities.

In our crystal structure of queuine-bound murine TGT, the cyclopentenediol moiety of the ligand is embedded between loops β4α4 and β6α6 of QTRT1. The main chain of loop β6α6 superimposes nearly perfectly with that of the same loop in the crystal structure of $preQ_1$-bound *Z. mobilis* TGT (PDB entry 1P0E). In addition to the mentioned Leu230, Ser231 and Glu234, it contains residue

Gly232, which is invariant in QTRT1 subunits but replaced by a valine in far more than 90% of bacterial TGT enzymes which feature the $preQ_1$ base as physiological substrate. Clearly, the side chain of a valine residue at this position would implement a steric clash with the cycylopentenediol moiety of queuine. In contrast to loop β6α6, loop β4α4 in part takes a significantly different course compared to its counterpart in the bacterial enzyme to accomplish best possible shape complementarity to the substrate base. While Asp159 of QTRT1 and the equivalent Asp156 of *Z. mobilis* TGT are nearly congruent, both His160 and Val161 of QTRT1 are shifted away from the substrate base by ≈2 Å in comparison to the corresponding Glu157 and Cys158 from *Z. mobilis* TGT. This allows the isopropyl side chain of Val161, which is invariant in QTRT1, to establish Van-der-Waals contacts both to the aromatic scaffold and to the five-membered side chain ring of queuine (Figure 7C). In ≈90% of bacterial TGT enzymes, Val161 is replaced by cysteine. Indeed, there exists experimental evidence that the mutation of Val161 to cysteine does not only result in the reduced affinity of QTRT1 to queuine but, in particular, in strongly increased affinity to the $preQ_1$ base.[41] Yet, as mentioned, the recognition of the $preQ_1$ base by QTRT1 has to be avoided since its insertion into tRNA is irreversible and eukaryotes do not possess the enzymes required for its conversion to queuosine.

The Cα atom of Ser164 is, compared to that of the corresponding Tyr161 from *Z. mobilis* TGT, shifted towards the binding pocket by more than 2.5 Å. This allows the formation of a weak H bond (3.2 Å) between the main chain amide of Ser164 and the 4-hydroxyl group of the cycylopentenediol moiety of queuine. A further H bond (3.2 Å) is formed between the 4-hydroxyl group and the side chain hydroxyl of Ser164. However, it seems not very stable since in the crystal structure a second, alternative conformation is observed for the Ser164 hydroxyl group, which does not allow this interaction. Notably, Ser164 as well as the successive residue, Thr165, which are well-defined in the electron density map of the queuine-bound TGT structure, are omitted from the structural models of citrate-bound and apo-TGT, since there is no clear electron density assignable to these residues. Obviously, both residues adopt a well-defined conformation only upon the binding of queuine. The 5-

hydroxyl group of the queuine cyclopentenediol moiety is solvent-exposed in our structure and not involved in any specific interactions.

Using TEW as additive, we were able to co-crystallize murine TGT with queuine at pH 6.8 in the presence of PEG 1000 as precipitant. Yet, as the crystals of apo-TGT obtained under this condition, the resulting crystals diffracted to moderate resolution only. Nonetheless, we determined the corresponding crystal structure at a resolution of 2.60 Å with refinement resulting in R and R_{free} factors of 21.1% and 23.8%, respectively. Clearly, the substrate base is present in the same conformation and virtually identically bound as in the above-described crystal structure of the TGT·queuine complex. Solely, the minor quality of the electron density map does not unambiguously reveal the weak polar interaction between Ser164 and the 4-hydroxyl group of the cyclopentenediol moiety of queuine observed in the above mentioned structure. However, Ser164 as well as the two successive residues, Thr165 and Val166 are reasonably defined in the electron density map. In contrast, due to ill-defined electron density, these residues had to be omitted from the model of the apo-structure based on a crystal obtained under the same condition but in the absence of queuine.

Our crystal structures of murine TGT in complex with queuine do not provide an ostensible explanation for the importance of the double bond within its five-membered ring system for efficient recognition by the enzyme. As mentioned, while this manuscript was in preparation, Sievers et al. published the crystal structure of human TGT in complex with an RNA substrate.[34] Here, α helix A of QTRT1 (which adopts a loop conformation in the crystal structure of murine TGT) is considerably shifted into the direction of a potentially bound substrate base when compared to the crystal structures of murine and human QTRT1. The superposition of our crystal structure of the murine TGT·queuine complex with the crystal structure of RNA-bound human TGT suggests that, caused by this induced fit, the queuine substrate is deeply buried in and tightly enclosed by the binding pocket in the presence of tRNA. As a consequence, disregarding the hydroxyl groups of its cyclopentenediol moiety, it seems almost totally shielded from the surrounding solvent. Moreover, the RNA-triggered conformation of α helix A obviously enables Van-der-Waals interactions of the side chain of Val112

therein with the cycylopentenediol moiety of queuine. Notably, Val112 appears invariant in the catalytic subunit of eukaryotic TGT. In all bacterial TGTs of known sequence it is replaced by a more bulky residue supposed to generate unfavorable interactions with the substituent of a potentially bound queuine molecule. Accordingly, Val112 may constitute a specificity determinant of the nucleobase substrate which, hitherto, has escaped our notice.

CONCLUSION

Clearly, the functional heterodimer formed by the catalytic QTRT1 subunit and the non-catalytic QTRT2 subunit of eukaryotic TGT is by far not as stable as the functional homodimer constituting the bacterial TGT. In former work, we had shown for the latter that the exchange rate between subunits amounts to one per several hours.[35] In contrast, the eukaryotic functional QTRT1/QTRT2 heterodimer is at equilibrium with the QTRT2 homodimer and the QTRT1 monomer. The idea is obvious that the equilibrium between the quaternary structures of eukaryotic TGT subunits may have a regulatory meaning, since it may be modulated in the living cell. Although there is presently no actual hint to such a function, this issue has clearly to be addressed in forthcoming projects.

Curiously, the crystal structure of murine QTRT1 as well as all crystal structures of heterodimeric murine TGT determined in this study reveal the presence of an α helix inserted between β strand 1 and α helix 1 of QTRT1. This secondary structure element, which we have termed α helix 0, has not been observed in any other crystal structure of a TGT enzyme until now. It is normally replaced by a loop required for the stabilization of the homo- or heterodimer interface. Yet, α helix 0 does not seem to constitute a mere crystallographic artefact since our structures containing murine QTRT1 are based on varying crystal forms revealing completely different crystal packing. Nonetheless, for steric reasons, α helix 0 is not compatible with a bound RNA substrate and will likely rearrange to a loop at least upon tRNA binding. Accordingly, it may be doubted that it owns any physiological role.

One of the crystal forms of the murine TGT presented in this report relies on the polyoxotungstate TEW as additive, the second one requires the presence of citrate, which occupies and obviously stabilizes the active site. Although the crystals gained in the presence of TEW diffract to moderate resolution only, they turned out valuable for structure interpretation and reliability. Using a crystal gained in the presence of citrate we were able to determine a high-quality structure of murine TGT in complex with queuine. This structure, however, was obtained after soaking the nucleobase into a pre-existing crystal because co-crystallization under the respective condition turned out impossible. Since a pre-formed crystal lattice sometimes does not allow for the structural adaptation of the protein potentially required for proper ligand binding, soaking may lead to artificial, physiologically irrelevant binding poses.[27] Yet, we were able to co-crystallize murine TGT with queuine in the presence of TEW. Reassuringly, despite of moderate resolution, the resultant crystal structure reveals a binding pose of this nucleobase which does not significantly differ from that observed in the structure obtained by soaking.

Our crystal structures of murine TGT in complex with queuine show that Val161 of QTRT1 makes Van-der-Waals contacts both with the 7-deazapurine scaffold and the cyclopentenediol moiety of the nucleobase. This residue, which is invariant in the catalytic subunit of eukaryotic TGT, is replaced by cysteine in ≈90% of bacterial TGTs. In addition, Gly232 of QTRT1, which is devoid of any side chain, provides the space required for the accommodation of the queuine cyclopentenediol moiety in the binding pocket. This residue is invariant in eukaryotic QTRT1 too, but is replaced by a valine in more than 90% of bacterial TGTs, whose physiological substrate, the $preQ_1$ base, does not contain this bulky substituent. So far, both amino acid positions within the active center have been deemed the only determinants of the different nucleobase specificities of eukaryotic and bacterial TGTs. However, in previous work, we attempted to change the substrate specificity of *Z. mobilis* TGT to that of eukaryotic TGT by mutating Val233 therein to glycine and Cys158 to valine, which led to a variant of the enzyme which was still unable to use queuine as a substrate.[42]

Actually, Sievers et al. observed in their crystal structure of the human TGT in complex with RNA that RNA binding causes a considerable shift of α helix A within QTRT1 towards a potentially bound substrate base.[34] This indicates that only in the presence of tRNA the nucleobase binding pocket of TGT is fully accomplished. Indeed, the superposition of our crystal structure of the murine TGT·queuine complex with that of the human TGT·RNA complex strongly suggests that the induced fit triggered by tRNA binding brings Val112 within α helix A into Van-der-Waals contact with the cyclopentenediol moiety of a bound queuine molecule (Figure S13). Also Val112 is invariant in the QTRT1 subunits of eukaryotic TGT while in some 80% of bacterial TGTs it is replaced by a phenylalanine, although the corresponding position may be occupied by methionine (as in *Z. mobilis* TGT), tryptophan, tyrosine, leucine or histidine (in the order of descending frequency) as well. In any case, in bacterial TGT, Val112 of QTRT1 is replaced by a more bulky residue which might produce clashes or, at least, unfavorable interactions with the hydroxyl groups of the queuine substituent. Mutational studies will be necessary to show if the replacement of Val112 in eukaryotic QTRT1 by a more voluminous residue in bacterial TGT constitutes a further determinant of nucleobase specificity. In addition, it will require the high-resolution structure of a TGT·RNA complex with bound queuine to gain a complete picture of how the physiological substrate base is bound by the eukaryotic TGT enzyme. Ultimately, such a structure might clarify the importance of the double bond within the cyclopentenediol for potent substrate binding, which was observed by Farkas et al. almost four decades ago[38] and which has been confirmed in the present study.

Recently, Alqasem et al. have reported on experimental evidence that eukaryotic TGT operates via a sequential bi-bi mechanism in which queuine binds first followed by tRNA binding, base exchange, the release of excised guanine, and, finally, the release of queuine-containing tRNA.[43] However, our crystal structures of murine TGT and, in particular, the structure of human TGT in complex with an RNA substrate[34] preclude such a mechanism. Clearly, if queuine binds to the active site of the enzyme first, it will block the access of the tRNA substrate since guanine-34 therein and

queuine are accommodated by the same binding pocket. Undoubtedly, the reaction catalyzed by eukaryotic TGT follows a ping-pong mechanism identical to that proceeding in bacterial TGT.

The entirety of the so far available crystal structures of bacterial and eukaryotic TGTs allows the deduction of the following reaction mechanism (Figure 8A). After the tRNA substrate has bound to the enzyme, Asp279 of QTRT1 (murine QTRT1 numbering) nucleophilically attacks the C1´ atom of guanosine-34 via its side chain carboxyl group. Concurrent with ester formation this leads to the cleavage of the glycosidic bond. The crystal structures of TGT enzymes in complex with RNA determined by Xie et al.[15] and by Sievers et al.[34] definitely prove the existence of the resulting covalent TGT·tRNA intermediate complex. The S_N2 reaction formally generates a negative charge on the N9 atom of the excised guanine. However, due to the close-by negatively charged carboxylate of Asp105 it is not able to persist at this position. Hence, it is relocated to the guanine N7 atom via mesomerism, enabling N7 to accept a proton from an adjacent water molecule with the resulting hydroxide ion being stabilized by the main chain amides of Leu230 and Ser231. A corresponding water molecule is clearly visible at an equivalent position in the high-resolution crystal structure of *Z. mobilis* TGT determined in complex with guanine.[39] Subsequently, facilitated by a flip of the Leu230/Ser231 peptide bond involving the deprotonation of Glu234 (see above), queuine replaces both the hydroxide and the excised guanine N7 tautomer in the binding pocket. Ultimately, the negatively charged side chain carboxylate of Asp105 promotes the deprotonation of the N9 atom of queuine concomitant with the nucleophilic attack of N9 to the C1´-atom of ribose-34. As a result, accompanied by the release of the Asp279 side chain carboxylate, a glycosidic bond is formed by the anomeric carbon atom of ribose-34 and queuine. The proton which is detached from the queuine N9 atom during the second S_N2 reaction might not be transferred to the Asp105 carboxylate but to the N3 atom of the queuine 7-deazaguanine scaffold. Here, it leads to the formation of a guanidinium function, which is stabilized by the side chain carboxylate groups of Asp105 and Asp159. After the release of the queuine-34 containing tRNA this proton will be passed on to a water molecule of the surrounding solvent.

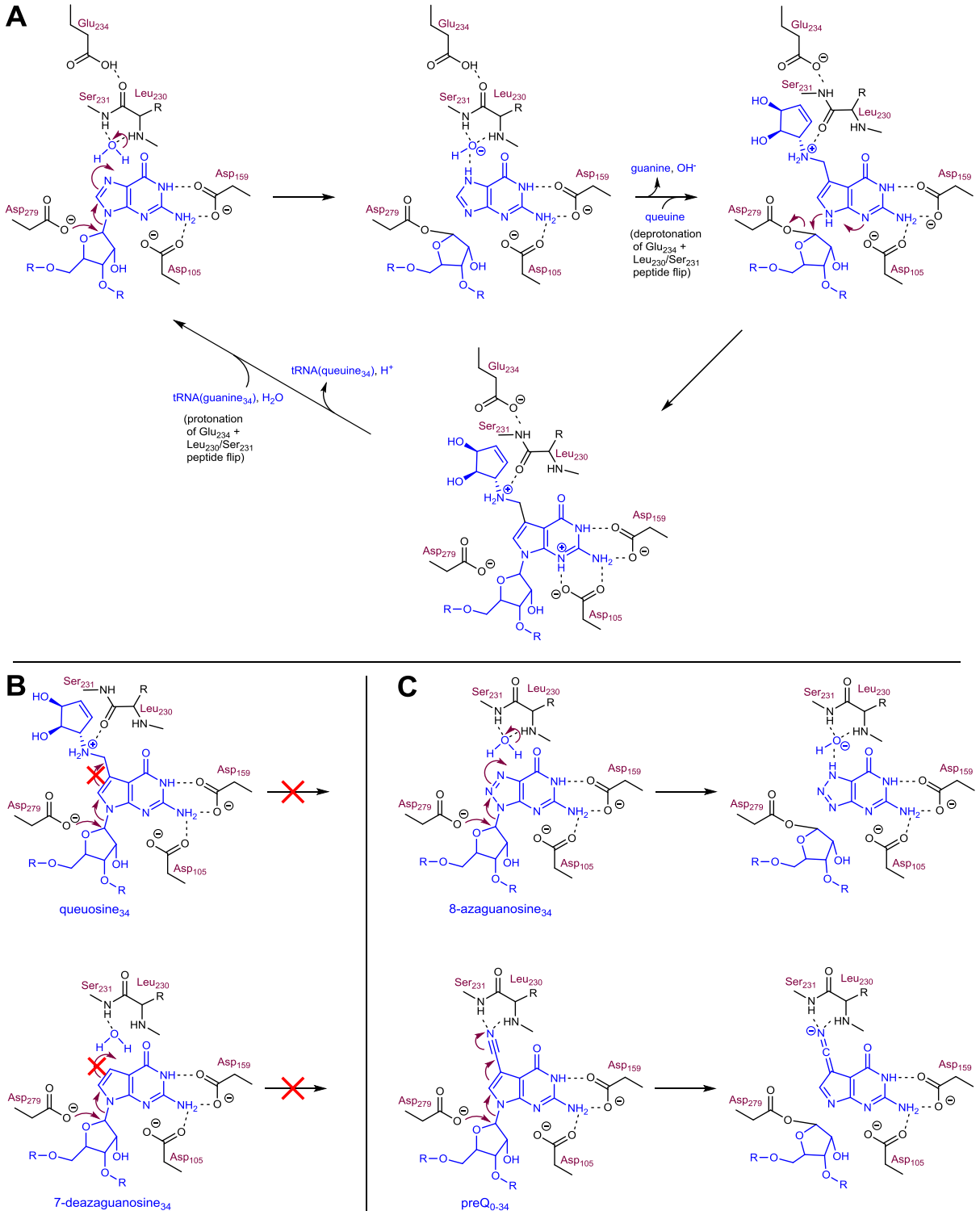

Figure 8. (A) Proposed ping pong mechanism of the TGT-catalyzed guanine-34/queuine exchange reaction as deduced from available TGT crystal structures (see main text). The mechanism involves the transfer of the negative charge, which is generated on guanine by the cleavage of the glycosidic bond, to a water molecule with the resulting hydroxide being stabilized by the main chain amides of Leu230 and Ser231. (B) This essential charge transfer is not possible in the case of 7-deazaguanosine or 7-aminomethyl derivatives thereof, which is why the TGT-catalyzed insertion of these nucleobases into tRNA occurs irreversibly. (C) 8-Azaguanine-34 may be cleaved off via the same mechanism as guanine-34. In contrast, the nitrile function of the $preQ_0$-34 base is able to directly accept the negative charge at a position where it is stabilized by the main chain amides of Leu230 and Ser231. The figure was generated via the program ChemDraw® (version 18.2.0.48).

The insertion of queuine into tRNA is irreversible since this base cannot be removed any more from the tRNA by a mechanism similar to that effecting the excision of guanine. To facilitate

the cleavage of the glycosidic bond within nucleoside-34, the concomitantly generated negative charge on N9 of the excised nucleobase has to be relocated to a position where it is stabilized by the main chain amides of Leu230 and Ser231. However, the substituent of queuine attached to the C7 atom of the 7-deazapurine scaffold does not allow for that (Figure 8B). In addition, the presence of queuine at position 34 of a TGT-bound tRNA causes a flip of the Leu230/Ser231 peptide bond concomitant with the deprotonation of the Glu234 side chain. As a consequence, the main chain amide of Ser231 is directed away from the binding pocket. Clearly, in this conformation it is unable to stabilize a nearby negative charge within the active center. For the same reasons, the insertion of further 7-(aminomethyl)-7-deazaguanine derivatives like the $preQ_1$ base,[37] dihydroqueuine[38] or NPPDAG[44] into tRNA occurs irreversibly. A further nucleobase, whose TGT-catalyzed insertion into tRNA was reported to be irreversible, is 7-deazaguanine.[38] Since its C7 atom is unsubstituted, its presence at position 34 of a TGT-bound tRNA still allows for the Leu230/Ser231 peptide bond conformation in which the Ser231 main chain amide forms an H bond with an interstitial water molecule. This, however, may not act as a proton donor, not least since the hydrogenation of the 7-deazaguanine C7 atom (accompanied by the oxidation of C8) would abolish the energetically favorable aromaticity of the 7-deazapurine scaffold (Figure 8B).

In contrast, the TGT-catalyzed insertion of 8-azaguanine and of the $preQ_0$ base into tRNA is fully reversible.[37,38,44] While 8-azaguanine-34 is excised from the tRNA via the same mechanism as guanine-34, the 7-substituent of $preQ_0$-34 does not allow the binding of a water molecule which might serve as a donor for re-protonation and, thus, as the final acceptor of the negative charge. Yet, the 7-nitrile substituent of $preQ_0$ is conjugated with the 7-deazapurine scaffold. Hence, via mesomerism, it is able to directly accept the negative charge originally generated on the N9 atom, rendering an interstitial water molecule unnecessary (Figure 8C). At the latest after its release from the enzyme, the excised negatively charged $preQ_0$ base will be protonated by a water molecule of the surrounding solvent.

METHODS

Gene Expression and Mutagenesis, Protein Production and Purification.

The recombinant, separately performed overexpression of murine *QTRT1* and *QTRT2* genes as well as the purification of the respective gene products was done as described by Behrens et al..[19] The site-directed mutagenesis of the *QTRT2* gene was carried out via the QuikChange Lightning kit (Agilent) according to the vendor´s instructions. For DNA manipulation, plasmids were prepared using the peqGOLD plasmid miniprep kit (PEQLAB). Required DNA primers were purchased from Eurofins MWG Operon. In each case, the complete gene was re-sequenced (by Eurofins MWG Operon) to confirm the presence of desired mutations and/or the absence of accidental mutations. Moreover, the molecular masses of QTRT1 and QTRT2 (variants) were measured to verify identity, integrity and homogeneity, each. They were in excellent agreement with the respective calculated molecular masses [calculated/measured: QTRT1: 44237 Da/44237 ± 3 Da; QTRT2: 47161 Da/47162 ± 1 Da; QTRT2(Ser41Ala): 47145 Da/47145 ± 1 Da; QTRT2(Tyr354Phe): 47145 Da/47144 ± 1 Da; QTRT2(Ser41Ala/Tyr354Phe): 47129 Da/47131 ± 3 Da].

For the dual expression of the *QTRT1* gene and the *QTRT2* gene, both codon-optimized genes[19] were (separately from each other) PCR-amplified with the codons encoding the N-terminal ten amino acids of QTRT1 (UniProtKB: Q9JMA2) and the codon encoding the N-terminal methionine of QTRT2 (UniProtKB: B8ZXI1) being omitted. Via the primers used for amplification, a *Strep*-tag II® encoding sequence followed by a sequence encoding a PreScission™ Protease cleavage site were fused in frame to the 5´ end of the *QTRT2* gene. A sequence encoding a PreScission™ Protease cleavage site was attached in frame to the 5´ end of the *QTRT1* gene too. The resulting reading frames were inserted into the multiple cloning sites 1 (*QTRT1*) and 2 (*QTRT2*) of the dual gene expression vector pETDuet-1 (NOVAGEN). In the case of the *QTRT1* gene, cloning was performed such that the sequence encoding the PreScission™ Protease cleavage site separated the target gene from a sequence encoding an N terminal His_6 tag originating from the pETDuet-1 vector (Figure S14). The re-

striction enzyme recognition sequences required for cloning were added to the termini of the respective inserts via the primers used for amplification too. The resultant plasmid allowing the combined expression of murine *QTRT1* and *QTRT2* genes was termed pETDuet-1-mTGT.

For the recombinant production of the heterodimeric murine TGT, pETDuet-1-mTGT was transformed into *Vibrio natriegens* Vmax™ Express (Synthetic Genomics). Transformed cells were grown at 37 °C in 2 L of 2 × YT medium (20 g L^{-1} yeast extract, 32 g L^{-1} Tryptone, 17 g L^{-1} NaCl, 0.2% glucose, 17.6 mmol L^{-1} Na_2HPO_4) containing 25 mg L^{-1} ampicillin in Erlenmeyer baffled flasks with the volume of the expression culture not exceeding ¼ of flask volume. As soon as an OD_{600} of ≈1.0 was reached, the bacterial culture was cooled to 15 °C and gene expression was induced by the addition of IPTG to a final concentration of 1 mmol L^{-1}. Incubation under vigorous shaking was continued at 15 °C for a period of 24 h, whereupon cells were harvested and frozen at -80 °C.

The frozen cell pellet was re-suspended in 150 mL of lysis buffer [100 mmol L^{-1} Tris-HCl (pH7.5), 150 mmol L^{-1} NaCl, and 1.0 mmol L^{-1} EDTA] at room temperature. Cell lysis occurred on ice in a Rosett glass jar by ultrasound for four times 4 min using a Branson Sonifier 250 endowed with a flat tip (output control 7, 30% duty cycle). Afterwards, the cell lysate was centrifuged at 50000 *g* and 4 °C for 60 min. The clear supernatant was loaded onto a *Strep*-Tactin® XT Superflow high capacity column (IBA) with a bed volume of 5 mL. The column was washed with 80 mL of lysis buffer followed by a wash step with 20 mL of lysis buffer plus 750 mmol L^{-1} LiCl (causing the partial removal of bound nucleic acids) and a final wash step with 50 mL of lysis buffer at a flow rate of 4.5 mL min^{-1}. Subsequently, the target protein was eluted from the column matrix with 30 mL of elution buffer [100 mmol L^{-1} TrisHCl (pH7.5), 150 mmol L^{-1} NaCl, 1.0 mmol L^{-1} EDTA, and 50 mmol L^{-1} biotin]. To cleave off both the (unused) His_6 tag from QTRT1 and the *Strep*-tag II® from QTRT2, 1 mg of PreScission™ Protease was added to the combined murine TGT containing fractions and incubated at 4 °C for 24 h. After 24 h, another 1 mg of PreScission™ Protease was added and the sample was incubated at 4 °C for another 24 h. Subsequently, the PreScission™ Protease (endowed with an N terminal GST tag) was removed by running the sample twice through a GSTrap™ Fast Flow column with a bed volume of 5 mL (Cytiva) with buff-

er W [100 mmol L^{-1} TrisHCl (pH 8.0), 150 mmol L^{-1} NaCl, and 1 mmol L^{-1} EDTA]. The flow rate during this step was set to 1 mL min^{-1}. The TGT containing flow through was transferred into a buffer containing 15 mmol L^{-1} TrisHCl (pH 7.5) and 1500 mmol L^{-1} NaCl and concentrated to a volume of ≈8 mL using a Vivaspin™ 20 centrifugal concentrator with 30 kDa cutoff (Sartorius). This sample was loaded onto a HiPrep™ 16/10 Phenyl High Performance column (Cytiva) for hydrophobic interaction chromatography. The column was washed with 35 mL of Phenyl-Sepharose™ binding buffer [15 mmol L^{-1} TrisHCl (pH 7.5) and 1500 mmol L^{-1} NaCl] to efficiently remove residual nucleic acid contaminants. Protein elution occurred with Phenyl-Sepharose™ elution buffer [15 mmol L^{-1} TrisHCl (pH 7.5) and 25 mmol L^{-1} NaCl] using a linear gradient comprising 35 mL from 0% to 100% elution buffer. Flow rate during hydrophobic interaction chromatography was adjusted to 3 mL min^{-1}. All chromatographic steps were carried out at room temperature using an ÄKTA purifier LC system (GE Healthcare Bio-Sciences AB). For crystallization and/or storage, fractions containing virtually pure TGT were concentrated to a mass concentration of ≈7.5 mg mL^{-1} using a Vivaspin™ 20 centrifugal concentrator (30 kDa cutoff). Concomitantly, buffer was exchanged by 15 mmol L^{-1} HEPES (pH 7.5), 150 mmol L^{-1} NaCl, and 2 mmol L^{-1} DTT. The yield achieved by this protocol typically amounted to ≈9 mg TGT per L of bacterial culture. Compared to the original murine TGT, the first ten amino acid residues are replaced by the sequence Gly-Pro in the recombinant QTRT1 subunit, while in the recombinant QTRT2 subunit solely the N terminal methionine is replaced by Gly-Pro. The complete removal of the *Strep*-tag II® from QTRT2 and of the His_6 tag from QTRT1 was verified by means of mass spectrometry (mass spectrometry facility of the Philipps University of Marburg). The measured molecular masses of QTRT1 and QTRT2 amounted to 43375 and 46310 Da, respectively, which is in excellent agreement with the calculated molecular masses of the recombinant proteins (43377 and 46311 Da, respectively).

Determination of Kinetic Parameters and K_i Values.

The determination of Michaelis-Menten parameters of murine TGT was done by monitoring the insertion of ^{3}H-labelled guanine (7.5% [8-^{3}H]-guanine, 20 Ci $mmol^{-1}$, American Radiolabeled Chemicals, Inc.) into in vitro transcribed tRNA as described by Biela et al..[42] For the determination of

K_m(tRNA^{Tyr}), the concentration of [^{3}H]-labelled guanine was kept constant at 10 µmol·L^{-1} while the concentration of tRNA^{Tyr} varied between 0.26 µmol·L^{-1} and 15 µmol·L^{-1}. In order to determine K_m(guanine) the concentration of [^{3}H]-labelled guanine was varied between 0.26 µmol L^{-1} and 15 µmol L^{-1} with the concentration of tRNA^{Tyr} being fixed at 6 µmol L^{-1}. Kinetic parameters were calculated using the program *GraphPad PRISM* (version 7.04).

The determination of k_{cat} values for non-radiolabeled substrate bases occurred via a "washout assay" monitoring the loss of [8-^{3}H]-guanine from tRNA^{Tyr} radiolabeled in position 34. Here, the concentration of tRNA^{Tyr}([8-^{3}H]-guanine-34) was kept constant at 6 µmol L^{-1}. Substrate bases were used at saturating concentration, each (guanine, queuine, preQ$_0$ base, and 8-azaguanine: 20 µmol L^{-1}; dihydroqueuine and NPPDAG: 50 µmol L^{-1}; preQ$_1$ base: 100 µmol L^{-1}). K_i values were determined as described by Grädler et al.[45] with the concentrations of [8-^{3}H]-guanine and tRNA^{Tyr} amounting to 1.5 µmol L^{-1} and 6 µmol L^{-1}, respectively.

In each assay, the murine TGT enzyme was used at a concentration of 37.5 nmol L^{-1}. Unmodified *E. coli* tRNA^{Tyr} (ECY2)[46] was synthesized via in vitro transcription by T7-RNA-Polymerase and purified as described by Nguyen et al..[35] The enzymatic radiolabeling of tRNA^{Tyr} occurred as described by Tidten et al.[39] using 7.5% [8-^{3}H]-guanine (20 Ci mmol^{-1}, American Radiolabeled Chemicals, Inc.). The preQ$_1$ base and queuine were synthesized as described by Gerber and Klebe.[47] NPPDAG was prepared following the procedure published by Varghese et al..[23] The preQ$_0$ base was prepared according to a protocol by Migawa et al..[48] Dihydroqueuine was synthesized via catalytic hydrogenation of the synthetic cyclohexylidene-protected precursor of queuine, prior to that obtained by a known literature procedure[47] and by final deprotection as detailed in the Supporting Information ("Synthesis of dihydroqueuine").

Size Exclusion Chromatography Coupled to Native Mass Spectrometry.

Size Exclusion Chromatography coupled with native Mass Spectrometry (SEC-nMS) was set up using an Acquity UPLC H-Class system (Waters, Manchester, UK) including a quaternary solvent manager, a sample manager set at 10 °C, a column oven and a TUV detector operating at 280 nm and

214 nm. This system was hyphenated to a Synapt G2 HDMS mass spectrometer (Waters, Manchester, UK). An Acquity BEH SEC 200 Å, 1.7 µm, 2.1 × 150 mm column (Waters, Manchester, UK) was used, with an isocratic elution of 500 mmol L^{-1} ammonium acetate (pH 8.0) at a constant flow rate of 100 µL min^{-1} over 10 min.

The Synapt G2 HDMS was operated in the positive mode with a capillary voltage of 3.0 kV. The sample cone and pressure in the interface region were set to Vc = 100 V and Pi = 6 mbar, respectively. Acquisitions of mass spectra were carried out over m/z range 1000 to 15 000 mass range with a 1.5 s scan time. External calibration was performed using singly charged ions produced by a 2 g L^{-1} solution of cesium iodide in 2-propanol/water (50/50 v/v). MS data interpretations were performed using Mass Lynx V4.1 (Waters, Manchester, UK).

5 µL of protein solutions at 36 µmol L^{-1} of QTRT1 WT, QTRT2 WT and the different mutants of QTRT2 [QTRT2(S41A), QTRT2(Y354F) and QTRT2(S41A-Y354F)] were injected individually to determine the oligomeric state of the proteins. Then, equimolar mixtures of the different mutants with QTRT1 were analyzed under similar experimental and instrumental conditions after 5 min reaction time, to assess the relative intensities of heterodimers and the unbound QTRT1. The relative intensity of monomeric QTRT1 for each individual equimolar mixture was calculated upon integration of the area underneath of both SEC peaks. The heterodimer/homodimer ratio was calculated from MS data. In this case, the three most intense MS peaks corresponding to each population were considered to calculate the relative intensity of homodimeric and heterodimeric species. It is worth to notice that both measurements, the relative intensity of unbound QTRT1 as well as the heterodimer ratio, were performed in triplicate for each individual equimolar mixture under strictly the same experimental and instrumental conditions.

Crystallization, Data Collection, Structure Determination, Model Building and Refinement.

All crystals of QTRT1 and of the QTRT1/QTRT2 heterodimer were produced via the sitting-drop vapor diffusion method in the presence of 500 µL reservoir solution at 18 °C. In each case, crystals grew after a few days. For the crystallization of murine QTRT1, 2 µL of protein solution [≈10 g L^{-1} in 20 mmol L^{-1} HEPES (pH 7.5), 1000 mmol L^{-1} NaCl, 2 mmol L^{-1} DTT] were mixed with 2 µL of reservoir solution [100 mmol L^{-1} CAPS (pH 10.5), 200 mmol L^{-1} NaCl, 20% (w/V) PEG 8000]. Prior to data collection, crystals were transferred to reservoir solution containing 30% (V/V) glycerol as cryo-protectant for a few seconds and vitrified in liquid nitrogen.

For the crystallization of the QTRT1/QTRT2 heterodimer, 2 µL of protein solution [≈7.5 g L^{-1} in 15 mmol L^{-1} HEPES (pH 7.5), 150 mmol L^{-1} NaCl, 2 mmol L^{-1} DTT] were mixed with 2 µL of reservoir solution A [100 mmol L^{-1} Na/K phosphate (pH 6.8), 200 mmol L^{-1} NaCl, 14% (w/v) PEG 1000, 1 mmol L^{-1} $Na_6[TeW_6O_{24}]$ (TEW; Jena Bioscience)] or reservoir solution B [100 mmol L^{-1} sodium citrate (pH 5.9), 700 mmol L^{-1} $(NH_4)_2SO_4$, 1000 mmol L^{-1} Li_2SO_4]. Prior to data collection, crystals were transferred to a buffer composed of 75% solution A or B and 25% glycerol or PEG 200 (V/V) as cryo-protectant, respectively. After about 2 min, they were vitrified in liquid nitrogen. For the co-crystallization of murine TGT with queuine using reservoir solution A (containing TEW), the ligand was added to the crystallization solution at a concentration of 0.5 mmol L^{-1}. To vitrify the crystal of the TGT·queuine complex for data collection, it was transferred to cryo-buffer [75% solution A plus 25% glycerol (V/V)] containing the ligand at a concentration of 0.5 mmol L^{-1}. To obtain crystals of apo-TGT in the absence of TEW, crystals gained with reservoir solution B were transferred to buffer C [100 mmol L^{-1} MES (pH 5.9), 700 mmol L^{-1} $(NH_4)_2SO_4$, 1000 mmol L^{-1} Li_2SO_4] for 2 min to remove the citrate from the substrate binding pocket. Prior to data collection, vitrification took place in a buffer composed of 75% solution C and 25% PEG 200 (V/V). To generate crystals of the TGT·queuine complex in the absence of TEW, apo-TGT crystals were soaked in a solution composed of 92% solution C and 8% 100 mmol L^{-1} queuine dissolved in DMSO (V/V) for 10 min. Subsequent vitrification occurred in a solution com-

posed of 67% solution C, 8% 100 mmol L^{-1} queuine dissolved in DMSO, and 25% PEG 200 (V/V/V). Diffraction data were collected at 100 K at the Helmholtz-Zentrum Berlin, BESSY II MX-beamline BL14.1 and the wavelengths that are listed in Table S1. All diffraction images were indexed, processed and scaled using *XDSAPP2.0*.[49] Data collection and refinement statistics are summarized in Table S1.

The QTRT1 structure was determined from a two wavelengths MAD experiment using the anomalous scattering of the naturally bound zinc ion. The used wavelengths were 1.282814 Å (peak) and 1.283345 Å (inflection point). Exhibiting a solvent content of 56.7%, which results in a Matthews coefficient of 2.84 $Å^3$ Da^{-1}, the crystal contains two polypeptide chains within the asymmetric unit. The determination of the two Zn^{2+} positions, the calculation of initial phases, density modification and subsequent auto-tracing was done via the *Phenix* AutoSol wizard[50] using default settings. The dataset collected at a wavelength of 1.282814 Å was used for refinement using the program *Phenix*[51] with intermittent cycles of model building in Coot.[52] Translation/Libration/Screw-rotation (TLS) refinement involving the partitioning of the model into groups defined by the program and non-crystallographic symmetry restraints were applied in every cycle of *Phenix*. The *B* values for all atoms were refined isotropically.

All structures of the QTRT1/QTRT2 heterodimer were determined via molecular replacement using the program *Phaser*[53] from the *CCP4* suite.[54] The crystal structures of murine QTRT1 (PDB entry 6H62) and of murine QTRT2 (PDB entry 6FV5) (one chain from each) were used as search models. Initial simulated annealing (Cartesian) occurred via *Phenix*.[51,55] Subsequent refinement was done with *Phenix* with intermittent cycles of model building in Coot.[52] In each case, *xyz* coordinates (reciprocal space) and the occupancies of atoms with an occupancy unequal 100% were refined. In the case of TEW containing structures, *B* values were refined in groups, while in the case of the remaining structures, the *B* values for all atoms were refined individually and isotropically. TLS refinement involving the partitioning of the model into five groups per protein chain defined by the program was applied in addition.

Hydrogen atoms were not added to any structure, since in no case this did result in any improvement of the *R* value. The crystallographic information (cif) files of the organic ligands (except queuine) were prepared using the Grade Web Server (http://grade.globalphasing.org/cgi-bin/grade/server.cgi). For the inorganic polyoxometallates, cif files were generated by means of the eLBOW module of *Phenix*[55,56] using the coordinate files[31,32] without further optimization. The structure of queuine was generated by the program *MOE* ("Molecular Operating Environment" 2019.01; Chemical Computing Group ULC) using the force field mmff94x. Ligands and alternative conformations were only incorporated if the corresponding occupation amounted to at least 20%. Water molecules were either incorporated at 100% occupancy or at 50% occupancy if the particular water molecule corresponded to an alternative conformation of a side chain.

Figure Preparation.

Structural figures were prepared using *Pymol* (http://www.pymol.org).

Protein Data Bank Accession Codes.

Coordinates and structure factors have been deposited under following accession codes: murine QTRT1: 6H62; murine TGT crystallized with TEW: 7OVS; murine TGT with bound queuine, crystallized with TEW: 7OWZ; murine apo-TGT: 7OV9; murine TGT with bound citrate: 7B2I; murine TGT with bound queuine: 7OVO.

FUNDING

We acknowledge support and travel grant to the BESSY II synchrotron provided by the Helmholtz-Zentrum Berlin, Germany. This work was supported by the CNRS, the University of Strasbourg, the “Agence Nationale de la Recherche” and the French Proteomic Infrastructure (ProFI; ANR-10-INBS-08-03). The authors would like to thank GIS IBiSA and Région Alsace for financial support in purchasing a Synapt G2 HDMS instrument. R. B. acknowledges the Innovative Training Network “Targeted Anti-Cancer Therapies” (TACT) from the MARIE SKLODOWSKA-CURIE ACTIONS (H2020-MSCA-ITN-2018) for the funding of her PhD project.

SUPPORTING INFORMATION

TGT sequence alignment (Figure S1); Supporting structural Figures S2–S7 and S12-S13; Enzyme kinetics data (Figures S8-S11); Construction of mQTRT1/mQTRT2 co-expression plasmid (Figure S14); Details to the synthesis of dihydroqueuine; Crystallographic Table S1.

ACKNOWLEDGEMENTS

We gratefully acknowledge the beamline staff at BESSY II (Helmholtz-Zentrum Berlin, Germany) for outstanding support during data collection and C. Sohn for his help during in-house X-ray data collection. In particular, we thank A. Bijelic for his invaluable help in identifying the Strandberg-type polyoxotungstate in the crystal structure of murine TGT crystallized in the presence of TEW. Not least, we thank K. Sievers and R. Ficner for providing us with the coordinates and structure factors of the human TGT·RNA complex prior to publication.

REFERENCES

1. Tuorto, F.; Legrand, C.; Cirzi, C.; Federico, G.; Liebers, R.; Müller, M.; Ehrenhofer-Murray, A. E.; Dittmar, G.; Gröne, H.-J.; Lyko, F. Queuosine-modified tRNAs confer nutritional control of protein translation. *EMBO J.* **2018**, *37*, e99777.

2. Wang, X.; Matuszek, Z.; Huang, Y.; Parisien, M.; Dai, Q.; Clark, W.; Schwartz, M. H.; Pan, T. Queuosine modification protects cognate tRNAs against ribonuclease cleavage. *RNA* **2018**, *24*, 1305-1313.

3. Müller, M.; Hartmann, M.; Schuster, I.; Bender, S.; Thüring, K. L.; Helm, M.; Katze, J. R.; Nellen, W.; Lyko, F.; Ehrenhofer-Murray, A. E. Dynamic modulation of Dnmt2-dependent tRNA methylation by the micronutrient queuine. *Nucleic Acids Res.* **2015**, *43*, 10952-10962.

4. Phillips, G.; Yacoubi, B. E.; Lyons, B.; Alvarez, S.; Iwata-Reuyl, D.; de Crécy-Lagard, V. Biosynthesis of 7-deazaguanosine-modified tRNA nucleosides: a new role for GTP cyclohydrolase I. *J. Bacteriol.* **2008**, *190*, 7876-7884.

5. McCarty, R. M.; Somogyi, Á.; Bandarian, V. *Escherichia coli* QueD is a 6-carboxy-5,6,7,8-tetrahydropterin synthase. *Biochemistry* **2009**, *48*, 2301-2303.

6. McCarty, R. M.; Somogyi, Á.; Lin, G.; Jacobsen, N. E.; Bandarian, V. The deazapurine biosynthetic pathway revealed: in vitro enzymatic synthesis of $preQ_0$ from guanosin 5´-triphosphate in four steps. *Biochemistry* **2009**, *48*, 3847-3852.

7. McCarty, R. M.; Krebs, C.; Bandarian, V. Spectroscopic, steady-state kinetic, and mechanistic characterization of the radical SAM enzyme QueE, which catalyzes a complex cyclization reaction in the biosynthesis of 7-deazapurines. *Biochemistry* **2013**, *52*, 188-198.

8. Van Lanen, S. G.; Reader, J. S.; Swairjo, M. A.; de Crécy-Lagard, V.; Lee, B.; Iwata-Reuyl, D. From cyclohydrolase to oxidoreductase: discovery of nitrile reductase activity in a common fold. *Proc. Natl. Acad. Sci. USA* **2005**, *102*, 4264-4269.

9. Okada, N.; Nishimura, S. Isolation and characterization of a guanine insertion enzyme, a specific tRNA transglycosylase, from *Escherichia coli*. *J. Biol. Chem.* **1979**, *254*, 3061-3066.

10. Van Lanen, S. G.; Kinzie, S. D.; Matthieu, S.; Link, T.; Culp, J.; Iwata-Reuyl, D. tRNA modification by S-adenosylmethionine:tRNA ribosyltransferase-isomerase. *J. Biol. Chem.* **2003**, *278*, 10491-10499.

11. Grimm, C.; Ficner, R.; Sgraja, T.; Haebel, P.; Klebe, G.; Reuter, K. Crystal structure of *Bacillus subtilis* S-adenosylmethionine:tRNA ribosyl transferase-isomerase. *Biochem. Biophys. Res. Commun.* **2006**, *351*, 695-701.

12. Greenhalgh, E. D.; Kincannon, W.; Bandarian, V.; Brunold, T. C. Spectroscopic and computational investigation of the epoxyqueuosine reductase QueG reveals intriguing similarities with the reductive dehalogenase PceA. **2022**, *Biochemistry 61*, 195-205.

13. Li, Q.; Zallot, R.; MacTavish, B. S.; Montoya, A.; Payan, D. J.; Hu, Y.; Gerlt, J. A.; Angerhofer, A.; de Grécy-Lagard, V.; Bruner, S. D. Epoxyqueuosine reductase QueH in the biosynthetic pathway to tRNA queuosine is a unique metalloenzyme. *Biochemistry* **2021**, *60*, 3152-3161.

14. Romier, C.; Reuter, K.; Suck, D.; Ficner, R. Crystal structure of tRNA-guanine transglycosylase: RNA modification by base exchange. *EMBO J.* **1996**, *15*, 2850-2857.

15. Xie, W.; Liu, X.; Huang, R. H. Chemical trapping and crystal structure analysis of a catalytic tRNA guanine transglycosylase covalent intermediate. *Nat. Struct. Mol. Biol*. **2003**, *10*, 781-788.

16. Ritschel, T.; Atmanene, C.; Reuter, K.; Van Dorsselaer, A.; Sanglier-Cianferani. S; Klebe, G. An integrative approach combining noncovalent mass spectrometry, enzyme kinetics and X-ray crystallography to decipher Tgt protein-protein and protein-RNA interaction. *J. Mol. Biol.* **2009**, *393*, 833-847.

17. Boland, C.; Hayes, P.; Santa-Maria, I.; Nishimura, S.; Kelly, V. P. Queuosine formation in eukaryotic tRNA occurs via a mitochondria-localized heterodimeric transglycosylase. *J. Biol. Chem.* **2009**, *284*, 18218-18227.

18. Chen, Y.-C.; Kelly, V. P.; Stachura, S.; Garcia, G. Characterization of the human tRNA-guanine transglycosylase: confirmation of the heterodimeric subunit structure. *RNA* **2010**, *16*, 958-968.

19. Behrens, C.; Biela, I.; Petiot-Bécard, S.; Botzanowski, T.; Cianférani, S.; Sager, C. P.; Klebe, G.; Reuter, K. Homodimer architecture of QTRT2, the noncatalytic subunit of the eukaryotic tRNA-guanine transglycosylase. *Biochemistry* **2018**, *57*, 3953-3965.

20. Johannsson, S.; Neumann, P.; Ficner, R. Crystal structure of the human tRNA guanine transglycosylase catalytic subunit QTRT1. *Biomolecules* **2018**, *8*, 81.

21. Durand, J. M. B.; Okada, N.; Tobe, T.; Watarai, M.; Fukuda, I.; Suzuki, T.; Nakata, N.; Komatsu, K.; Yoshikawa, M.; Sasakawa, C. *vacC*, a virulence-associated chromosomal locus of *Shigella flexneri*, is homologous to *tgt*, a gene encoding tRNA-guanine transglycosylase (Tgt) of *Escherichia coli* K-12. *J. Bacteriol.* **1994**, *176*, 4627-4634.

22. Rakovich, T.; Boland, C.; Bernstein, I.; Chikwana, V. M.; Iwata-Reuyl, D.; Kelly, V. P. Queuosine deficiency in eukaryotes comprises tyrosine production through increased tetrahydrobiopterin oxidation. *J. Biol. Chem.* **2011**, *286*, 19354-19363.

23. Varghese, S.; Cotter, M.; Chevot, F.; Fergus, C.; Cunningham, C.; Mills, K. H.; Connon, S. J.; Southern, J. M.; Kelly, V. P. In vivo modification of tRNA with an artificial nucleobase leads to full disease remission in an animal model of multiple sclerosis. *Nucleic Acids Res.* **2017**, *45*, 2029-2039.

24. Zhang J.; Lu, R.; Zhang, Y.; Matuszek, Z.; Zhang, W.; Xia, Y.; Pan, T.; Sun, J. tRNA queuosine modification enzyme modulates the growth and microbiome recruitment to breast tumors. *Cancers* **2020**, *12*, E628.

25. Nagaraja, S.; Cai, M. W.; Sun, J.; Varet, H.; Sarid, L.; Trebicz-Geffen, M.; Shaulov, Y.; Mazumdar, M.; Legendre, R.; Coppée, J.-Y. et al. Queuine is a nutritional regulator of *Entamoeba histolytica* response to oxidative stress and a virulence attenuator. *mBio* **2021**, *12*, e03549-20

26. Kulkarni, S.; Rubio, M. A. T.; Hegedűsová, E.; Ross, R. L.; Limbach, P. A.; Alfonzo, J. D.; Paris, Z. Preferential import of queuosine-modified tRNAs into *Trypososma brucei* mitochondrion is critical for organellar protein synthesis. *Nucleic Acids Res.* **2021**, *49*, 8247-8260.

27. Ehrmann, F. R.; Stojko, J.; Metz, A.; Debaene, F.; Barandun, L. J.; Heine, A.; Diederich, F.; Cianférani, S.; Reuter, K.; Klebe, G. Soaking suggests "alternative facts": only cocrystallization discloses major ligand-induced interface rearrangements of a homodimeric tRNA-binding protein indicating a novel mode-of-inhibition. *PLoS ONE* **2017**, *12*, e0175723.

28. Ehrmann, F. R.; Kalim, J.; Pfaffeneder, T.; Bernet, B.; Hohn, C.; Schäfer, E.; Botzanowski, T.; Cianférani, S.; Heine, A.; Reuter, K. et al. Swapping interface contacts in the homodimeric tRNA-guanine transglycosylase: an option for functional regulation. *Angew. Chem. Int. Ed.* **2018**, *57*, 10085-10090.

29. Nguyen, D.; Abdullin, D.; Heubach, C. A.; Pfaffeneder, T.; Nguyen, A.; Heine, A.; Reuter, K.; Diederich, F.; Schiemann, O.; Klebe, G. Unraveling a ligand-induced twist of a homodimeric enzyme by pulsed-electron-electron double resonance. *Angew. Chem. Int. Ed.* **2021**, *60*, 23419-23426.

30. Jakobi, S.; Nguyen, T. X. P.; Debaene, F.; Metz, A.; Sanglier-Cianférani, S.; Reuter, K.; Klebe, G. Hot-spot analysis to dissect the functional protein-protein interface of a tRNA-modifying enzyme. *Proteins Struct. Funct. Bioinf.* **2014**, *82*, 2713-2732.

31. Bijelic, A.; Rompel, A. Ten good reasons for the use of the tellurium-centered Anderson-Evans polyoxotungstate in protein crystallography. *Acc. Chem. Res.* **2017**, *50*, 1441-1448.

32. Lin, B.-Z.; Li, Z.; Xu, B.-H.; He, L.-W.; Liu, X.-Z.; Ding, C. First Strandberg-type polyoxotungstate compound: Synthesis and characterization of organic-inorganic hybrid $(H_2en)(Hen)_2[H_2P_2W_5O_{23}]\cdot 5.42H_2O$. *J. Mol. Struct.* **2006**, *825*, 87–92.

33. Jakobi, S.; Nguyen, T. X. P.; Debaene, F.; Cianférani, S.; Reuter, K.; Klebe, G. What glues a homodimer together: systematic analysis of the stabilizing effect of an aromatic hot spot in the protein-protein interface of the tRNA-modifying enzyme Tgt. *ACS Chem. Biol.* **2015**, *10*, 1897-1907.

34. Sievers, K.; Welp, L.; Urlaub, H.; Ficner, R. Structural and functional insights into human tRNA-guanine transglycosylase. *RNA Biol.* **2021**, *18*, 382-396.

35. Nguyen, A.; Nguyen, D.; Nguyen, T. X. P.; Sebastiani, M.; Dörr, S.; Hernandez-Alba, O.; Debaene, F.; Cianférani, S.; Heine, A.; Klebe, G. et al. The importance of charge in perturbing the aromatic glue stabilizing the protein-protein interface of homodimeric tRNA-guanine transglycosylase. *ACS Chem. Biol.* **2020**, *15*, 3021-3029.

36. Hoops, G. C.; Townsend, L. B.; Garcia, G. A. tRNA-guanine transglycosylase from *Escherichia coli*: structure-activity studies investigating the role of the aminomethyl substituent of the heterocyclic substrate $preQ_1$. *Biochemistry* **1995**, *34*, 15381-15387.

37. Okada, N.; Nogushi, S.; Kasai, H.; Shindo-Okada, N.; Ohgi, T.; Goto, T.; Nishimura, S. Novel mechanism of post-transcriptional modification of tRNA. *J. Biol. Chem.* **1979**, *254*, 3067-3073.

38. Farkas, W. R.; Jacobson, K. B.; Katze, J. R. Substrate and inhibitor specificity of tRNA-guanine ribosyltransferase. *Biochim. Biophys. Acta* **1984**, *781*, 64-75.

39. Tidten, N.; Stengl, B.; Heine, A.; Garcia, G. A.; Klebe, G.; Reuter, K. Glutamate versus glutamine exchange swaps substrate selectivity in tRNA-guanine transglycosylase: Insight into the regulation of substrate selectivity by kinetic and crystallographic studies. *J. Mol. Biol.* **2007**, *374*, 764-776.

40. Brenk, R.; Stubbs, M. T.; Heine, A.; Reuter, K.; Klebe, G. Flexible adaptations in the structure of the tRNA-modifying enzyme tRNA-guanine transglycosylase and their implications for substrate selectivity, reaction mechanism and structure-based drug design. *ChemBioChem* **2003**, *4*, 1066-1077.

41. Chen, Y.-C.; Brooks, A. F.; Goodenough-Lashua, D. M.; Kittendorf, J. D.; Showalter, H. D.; Garcia, G. Evolution of eukaryal tRNA-guanine transglycosylase: insight gained from the heterocyclic substrate recognition by the wild-type and mutant human and *Escherichia coli* tRNA-guanine transglycosylases. *Nucleic Acids Res.* **2011**, *39*, 2834-2844.

42. Biela, I.; Tidten-Luksch, N.; Immekus, F.; Glinca, S.; Nguyen, T. X. P.; Gerber, H.-D.; Heine, A.; Klebe, G.; Reuter, K. Investigation of specificity determinants in bacterial tRNA-guanine transglycosylase reveals queuine, the substrate of its eucaryotic counterpart, as inhibitor. *PLoS ONE* **2013**, *8*, e64240.

43. Alqasem, M. A.; Fergus, C.; Southern, J. M.; Connon, S. J.; Kelly, V. P. The eukaryotic tRNA-guanine transglycosylase enzyme inserts queuine via a sequential bi-bi mechanism. *Chem. Commun.* **2020**, *56*, 3915-3918.

44. Fergus, C.; Al-qasem, M.; Cotter, M.; McDonnell, C. M.; Sorrentino, E.; Chevot, F.; Hokamp, K.; Senge, M. O.; Southern, J. M.; Connon, S. J. et al. The human tRNA-guanine transglycosylase displays promiscuous nucleobase preference but strict tRNA specificity. *Nucleic Acids Res.* **2021**, *49*, 4877-4890.

45. Grädler, U.; Gerber, H.-D.; Goodenough-Lashua, D. M.; Garcia, G. A.; Ficner, R.; Reuter, K.; Stubbs, M. T.; Klebe, G. A new target for shigellosis: rational design and crystallographic studies of inhibitors of tRNA-guanine transglycosylase. *J. Mol. Biol.* **2001**, *306*, 455-467.

46. Curnow, A. W.; Kung, F.-L.; Koch, K. A.; Garcia, G. A. tRNA-guanine transglycosylase from *Escherichia coli*: gross tRNA structural requirements for recognition. *Biochemistry* **1993**, *32*, 5239-5246.

47. Gerber, H.-D.; Klebe, G. Concise and efficient syntheses of $preQ_1$ base, Q base and (*ent*)-Q base. *Org. Biomol. Chem.* **2012**, *10*, 8660-8668.

48. Migawa, M. T.; Hinkley, J. M.; Hoops, G. C.; Townsend, L. B. A. A two step synthesis of the nucleoside Q precursor 2-amino-5-cyanopyrrolo[2,3-*d*]pyrimidin-4-one ($preQ_0$). *Synth. Commun.* **1996**, *26*, 3317-3322.

49. Sparta, K. M.; Krug, M.; Heinemann, U.; Mueller, U.; Weiss, M. S. XDSAPP2.0. *J. Appl. Cryst.* **2016**, *49*, 1085-1092.

50. Terwilliger, T. C.; Adams, P. D.; Read, R. J.; McCoy, A. J.; Moriarty, N. W.; Grosse-Kunstleve, R. W.; Afonine, P. V.; Zwart, P. H.; Hung, L. W. Decision-making in structure solution using Bayesian estimates of map quality: the PHENIX AutoSol wizard. *Acta Crystallogr. D Struct. Biol.* **2009**, *65*, 582-601.

51. Afonine, P. V.; Grosse-Kunstleve, R. W.; Echols, N., Headd, J. J.; Moriarty, N. W.; Mustyakimov, M.; Terwilliger, T. C.; Urzhumtsev, A.; Zwart, P. H.; Adams, P. D. Towards automated crystallographic structure refinement with phenix.refine. *Acta Crystallogr., Sect. D: Biol. Crystallogr.* **2012** *68*, 352-367.

52. Emsley, P.; Lohkamp, B.; Scott, W. G.; Cowtan, K. Features and development of Coot. *Acta Crystallogr. D Struct. Biol.* **2010**, *66*, 486-501.

53. McCoy, A. J.; Grosse-Kunstleve, R. W.; Adams, P. D.; Winn, M. D.; Storoni, L. C.; Read, R. J. Phaser crystallographic software. *J. Appl. Cryst.* **2007**, *40*, 658-674.

54. Potterton, E.; Briggs, P.; Turkenburg, M.; Dodson, E. A graphical interface to the CCP4 program suite. *Acta Crystallogr. D Struct. Biol.* **2003**, *59*, 1131-1137.

55. Liebschner, D.; Afonine, P. V.; Baker, M. L.; Bunkoczi, G.; Chen, V. B.; Croll, T. I.; Hintze, B.; Hung, L. W.; Jain, S.; McCoy, A. J. et al. Macromolecular structure determination using X-rays, neutrons and electrons: recent developments in *Phenix*. *Acta Crystallogr. D Struct. Biol.* **2019**, *75*, 861-877.

56. Moriarty, N. W.; Grosse-Kunstleve, R. W.; Adams, P. D. Electronic Ligand Builder and Optimization Workbench (eLBOW): a tool for ligand coordinate and restraint generation. *Acta Crystallogr. D Struct. Biol.* **2009**, *65*, 1074–1080.

TOC Graphic